Harnessing the immunostimulatory properties of oncolytic reovirus for anticancer immunotherapy

Groeneveldt, P.C.

CHAPTER 3

Preinduced reovirus-specific T-cell immunity enhances the anticancer efficacy of reovirus therapy

Christianne Groeneveldt[1], Priscilla Kinderman[1], Jordi J. C. van Stigt Thans[1], Camilla Labrie[1], Lisa Griffioen[1], Marjolein Sluijter[1], Diana J. M. van den Wollenberg[2], Rob C. Hoeben[2], Joke M. M. den Haan[3], Sjoerd H. van der Burg[1], Thorbald van Hall[1], Nadine van Montfoort[4#]

[1] Department of Medical Oncology, Oncode Institute, Leiden University Medical Center, 2333 ZA, Leiden, The Netherlands

[2] Department of Cell and Chemical Biology, Leiden University Medical Center, 2300 RC, Leiden, The Netherlands

[3] Department of Molecular Cell Biology and Immunology, Amsterdam University Medical Center, Cancer Center Amsterdam, Amsterdam Infection and Immunity Institute, Vrije Universiteit Amsterdam, Amsterdam, The Netherlands

[4] Department of Gastroenterology and Hepatology, Leiden University Medical Center, 2333 ZA, Leiden, The Netherlands

[#] Corresponding author

Journal for ImmunoTherapy of Cancer 2022;10:e004464. doi:10.1136/jitc-2021-004464

ABSTRACT

Background. Many solid tumors do not respond to immunotherapy due to their immunologically cold tumor microenvironment (TME). We and others found that oncolytic viruses, including reovirus type 3 Dearing, can enhance the efficacy of immunotherapy by recruiting $CD8^+$ T cells to the TME. A significant part of the incoming $CD8^+$ T cells is directed towards reovirus itself, which may be detrimental to the efficacy of OVs. However, here we aim to exploit these incoming virus-specific T cells as anticancer effector cells.

Methods. We performed an in-depth characterization of the reovirus-induced T-cell response in immune-competent mice bearing pancreatic KPC3 tumors. The immunodominant $CD8^+$ T-cell epitope of reovirus was identified using epitope prediction algorithms and peptide arrays, and the quantity and quality of reovirus-specific T cells after reovirus administration were assessed using high dimensional flow cytometry. A synthetic long peptide (SLP)-based vaccination strategy was designed to enhance the intratumoral frequency of reovirus-specific $CD8^+$ T cells.

Results. Reovirus administration did not induce tumor-specific T cells but rather induced high frequencies of reovirus-specific $CD8^+$ T-cell response directed to the immunodominant epitope. Priming of reovirus-specific T cells required a low-frequent population of cross-presenting dendritic cells which was absent in *Batf3*$^{-/-}$ mice. While intratumoral and intravenous reovirus administration induced equal systemic frequencies of reovirus-specific T cells, reovirus-specific T cells were highly enriched in the TME exclusively after intratumoral administration. Here, they displayed characteristics of potent effector cells with high expression of KLRG1, suggesting they may be responsive against local reovirus-infected cells. To exploit these reovirus-specific T cells as anticancer effector cells, we designed an SLP-based vaccination strategy to induce a strong T-cell response before virotherapy. These high frequencies of circulating reovirus-specific T cells were reactivated upon intratumoral reovirus administration and significantly delayed tumor growth.

Conclusions. These findings provide proof of concept that oncolytic virus-specific T cells, despite not being tumor-specific, can be exploited as potent effector cells for anticancer treatment when primed before virotherapy. This is an attractive strategy for low-immunogenic tumors lacking tumor-specific T cells.

GRAPHICAL ABSTRACT

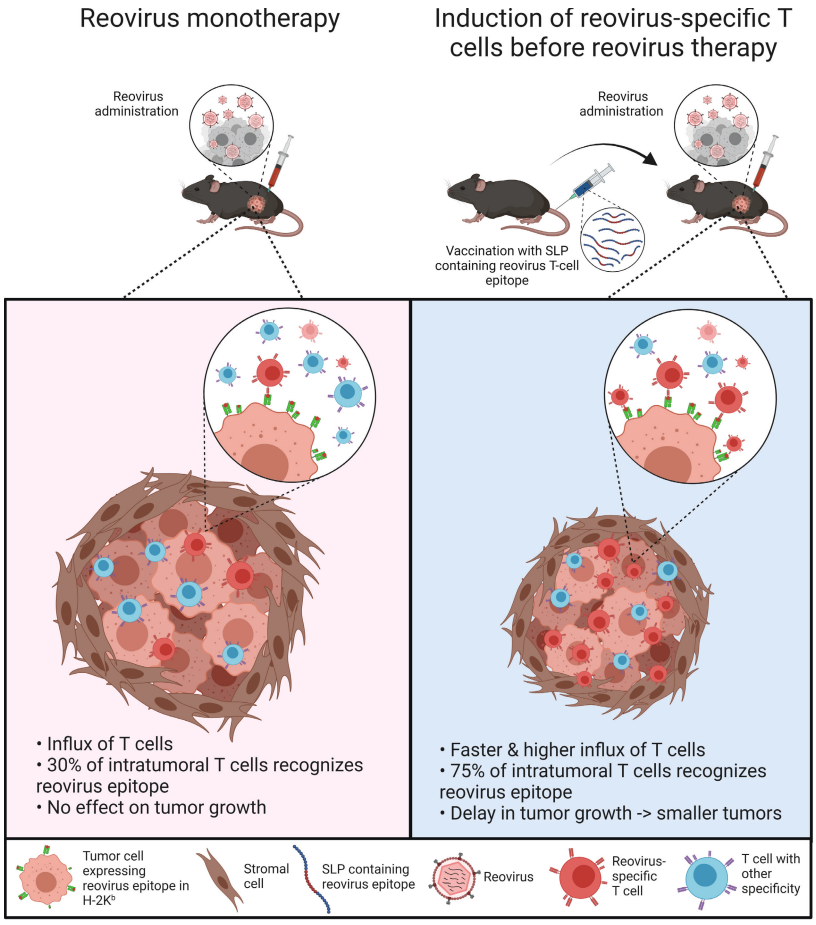

INTRODUCTION

Oncolytic viruses (OVs) are increasingly recognized as potent anticancer agents due to their preferential replication in cancerous cells and stimulation of host antitumor immunity (1). The mammalian reovirus type 3 Dearing strain (T3D) is one of the leading oncolytic viruses under clinical evaluation and displays an excellent safety record in clinical trials (2,3). Reoviruses show an inherent preference for replication in and lysis of transformed, but not healthy cells (4-6). As a monotherapy, reovirus has demonstrated moderate antitumor efficacy, for example in prostate xenograft models and prostate cancer patients (7,8). Recent advances in the field have shown that beyond their oncolytic capacity, OVs are useful as potent immunostimulatory agents. For example, they can enhance the efficacy of immune checkpoint blockade in immunogenic tumors by further enhancing the intratumoral density of tumor-specific $CD8^+$ T cells that can be reinvigorated by checkpoint blockade (1,9,10).

We questioned whether the immunostimulatory properties of OVs can also be beneficial for non-immunogenic tumors that lack tumor-specific T cells and thus are completely non-responsive to immune checkpoint therapy. We recently demonstrated that intratumoral reovirus administration strongly enhances the infiltration of $CD8^+$ T cells in a non-immunogenic murine pancreatic cancer model (11). A large proportion of these tumor-infiltrating lymphocytes (TILs) did not recognize the tumor but was directed towards reovirus itself. *Despite* being reovirus-specific, these T cells could be exploited by CD3-bispecific antibodies (CD3-bsAbs) to induce tumor regressions of established tumors. Here, we aim to exploit the incoming T cells as anticancer effector cells *because* they are virus-specific.

For this aim, we first investigated the requirements for an effective reovirus-specific T-cell response. We mapped the reovirus T-cell epitope, which allowed us to specifically study the kinetics, distribution, and phenotype of reovirus-specific T cells. We demonstrated that *Batf3*-driven cDC1s are involved in the priming of reovirus-specific T cells and that intratumoral reovirus administration is not required for priming but is strongly preferred for an efficient intratumoral influx of reovirus-specific T cells. In the tumor, reovirus-specific T cells have a profound effector phenotype. Priming of these T cells using a vaccination strategy before intratumoral reovirus therapy strongly improved its antitumor effect.

Our findings provide proof of concept that the presence of a pre-installed pool of oncolytic virus-specific T cells, despite not being tumor-specific, can effectively delay tumor growth after OV therapy. Exploiting these virus-specific T cells during OV administration is an attractive strategy for low-immunogenic tumors that lack tumor-specific T cells.

MATERIAL & METHODS

Reovirus

The wild-type reovirus strain R124 (here referred to as Reo) was previously isolated from a heterogeneous reovirus Type 3 Dearing (T3D) stock (VR-824) obtained from the American Type Culture Collection (ATCC) by two rounds of plaque purification using HER911 cells (12). Reovirus mutant Jin-3 was isolated from JAM-A-deficient U118MG cells after passaging of the wild-type T3D strain R124 (12). All experiments were performed using cesium chloride (CsCl)-purified stocks as described earlier (11). The total amount of particles was calculated based on OD_{260} values where 1 OD equals $2.10x10^{12}$ reovirus particles/mL (13), and the infectious titer was quantified by plaque assay on HER911 cells (14).

Cell lines and culture

The murine pancreatic cancer cell line KPC3 is a low-passage derivate of a primary KPC tumor with mutant *p53* and *K-ras* from a female C57BL/6 mouse (11,15). All cells were cultured at 37 °C in a humidified atmosphere containing 5% CO_2 in Iscove's Modified Dulbecco's Medium (IMDM; Invitrogen) supplemented with 8% fetal calf serum (FCS; Bodinco, Alkmaar, The Netherlands), 2mM L-glutamine (Gibco), 100 µg/mL penicillin and 100 µg/mL streptomycin (Gibco). The tumor cell line TC1 expresses the HPV16-derived oncogenes E6 and E7 and activated Ras oncogene and was additionally cultured in the presence of 400 µg/ml Geneticin (G418; Life Technologies), 1% nonessential amino acids (Life Technologies), and 1 mM sodium pyruvate (Life Technologies) (16). The cell line TC1. B7 was retrovirally transduced to express high levels of co-stimulatory molecule CD86. The DC line D1 was originally obtained from P. Ricciardi-Castagnoli (University of Milano-Bicocca, Milan, Italy) (17). Fre.D^b and Fre.K^b cell lines are stable transfectants of the Fisher rat embryo (Fre) cell line (18). Cell lines were assured to be free of *Mycoplasma* by regular PCR analysis. Authentication of the cell lines was done by Short Tandem Repeat (STR) profiling (IDEXX BioAnalytics, Ludwigsburg, Germany) and cells of low passage number were used for all experiments.

Animal experiments

Male C57BL/6J mice (H-2^b) were purchased from Charles River Laboratories (France). Male and female *Batf3*-deficient mice (The Jackson Laboratory, USA) were bred at the animal facility of Amsterdam University Medical Center. Mice were housed in individually ventilated cages with no more than 5 mice/cage. After one week of acclimatization after transport, mice (6-8 weeks old) were inoculated with subcutaneous KPC3 or TC1 tumors as described before (11). Intratumoral reovirus administration was performed under isoflurane anesthesia by injection of $1x10^7$ plaque-forming units (pfu) of reovirus or PBS as a control in a volume of 30 µL PBS on 3 consecutive days unless otherwise indicated. Intravenous administration of reovirus after tumor challenge was performed by injection of $3x10^7$ pfu of reovirus in a total volume of 100 µL PBS in the tail vein. Intratumoral peptide injection was performed under isoflurane anesthesia by injection of 50 µg peptide in 30 µL PBS.

For vaccination experiments, naive male C57BL/6J mice received the reovirus-derived SLP (DKMRVLSVSPKYSDLLTYVDAYVGV) or the HPV E7-derived SLP (GQAEPDRAHYNIVTFCCKCDS) (GenScript, Leiden, The Netherlands) to induce reovirus- or HPV-specific T-cell immunity. 50 nmol SLP was mixed with 20 µg CpG (ODN1826; InvivoGen) and subcutaneously injected in the tail-base region in 50 µL PBS. This injection was repeated after 2 weeks to boost the efficacy of vaccination. For immunization experiments, mice were immunized by intravenously injecting $1x10^7$ pfu of reovirus in a volume of 100 µL PBS in the tail vein. This injection was repeated after 2 weeks. After vaccination or immunization, mice were engrafted with a subcutaneous KPC3 tumor ($1x10^5$ cells in 100 µL PBS/0.1% BSA) and received reovirus intratumorally as described.

When checkpoint blockade was applied, mice were treated on indicated days with intraperitoneal injections of 200 µg PD-L1-blocking antibody (clone 10F.9G2; GoInVivo™ Purified anti-mouse CD274 Antibody; BioLegend). To deplete $CD8^+$ T cells after vaccination, mice were injected with 50 µg anti-CD8 antibody (Clone 2.43; produced *in-house*). Depletion of $CD8^+$ T cells was verified by flow cytometry before mice received intratumoral reovirus injections.

To reduce the number of experimental animals, some research questions were addressed in one experiment, thereby sharing the control group. This is indicated in the respective figure legends. Cages were randomly allocated to a certain treatment group by an independent researcher and treatments were given in a different order each time. During all experiments, tumors were measured 3 times a week in 3 dimensions using a caliper, in a blinded manner concerning the experimental group. For intratumoral analysis experiments, mice were sacrificed at indicated days after treatment before organs and blood were collected. For experiments where tumor growth was the experimental outcome, mice were sacrificed when the tumor volume exceeded 1000 mm^3 or when ulceration occurred. Tumors were divided into representative parts, which were either snap-frozen in liquid N2 and stored at -80 °C until further analysis, or immediately processed to single cells suspensions for flow cytometry analysis.

Cell preparation and flow cytometry

Tumors, liver, lungs, spleens, and (TD)LNs were dissociated into a single-cell suspension as described before (11). Liver, blood, and splenocytes were incubated with red blood cell lysis buffer for 3 minutes at room temperature (RT) before use. All cells were incubated with Zombie AquaTM Fixable Viability Dye (Biolegend) in PBS for 20 minutes at RT followed by incubation with 2.4G2 FcR blocking antibodies (clone 2.4G2; BD Biosciences) in FACS buffer (PBS, 0.5% BSA, and 1% sodium azide) for 20 minutes on ice. If applicable, cells were incubated with Reo $\mu1_{133-140}$ tetramer conjugated to APC or the HPV $E7_{49-57}$ tetramer conjugated to PE (both generated *in-house*) for 1 hour at RT in FACS buffer, after which surface markers (**Table S1**) were added directly to the tetramer mixture for 30 minutes of incubation at RT. After completion of staining protocols,

samples were fixed in 1% paraformaldehyde and acquired using a BD LSRFortessa™ X20 4L cell analyzer (BD Biosciences, San Jose, CA, USA) at the Flow cytometry Core Facility (FCF) of Leiden University Medical Center (LUMC) in Leiden, Netherlands (https://www.lumc.nl/research/facilities/fcf). Data were analyzed using FlowJo™ Software Version 10 (Becton, Dickinson, and Company). Opt-SNE plots (19) were generated using standard settings in OMIQ data analysis software (Omiq, Inc. www.omiq.ai).

Generation of reovirus-specific T-cell bulk

To generate a reovirus-specific T-cell bulk, a KPC3-bearing C57BL/6J mouse was intratumorally injected with 10^7 pfu of reovirus on three consecutive days. 6 days after the last reovirus injection, the mouse was sacrificed by cervical dislocation and the spleen was harvested and processed to a single-cell suspension. After red blood cell lysis, $30x10^6$ splenocytes were co-cultured in culture medium supplemented with 50 mM β-mercaptoethanol for 4 hours with $1.5x10^8$ infectious reovirus particles, equaling a multiplicity of infection (MOI) of 5. Hereafter, splenocytes were washed and plated at 300.000 cells/well in a round-bottom 96-well plate. Bulk cultures were restimulated weekly with irradiated reovirus-infected TC1 cells (6000 RAD) and irradiated naive splenocytes (3000 RAD) as feeders. Initially, bulk cultures were sustained with recombinant IL-2 (10 CU/mL) and later supplemented with 5% (v/v) conditioned medium from Con A- and PMA-stimulated rat splenocytes (18). When necessary, cellular debris was removed by Ficoll-Paque density-gradient centrifugation following the manufacturer's instructions. The specificity of the T-cell bulk was initially assessed using intracellular cytokine staining.

Peptide prediction

Peptide prediction was performed using the NetMHC 4.0 Server (Technical University of Denmark). Sequences of all segments (S1-4, M1-3, and L1-3, **Table S2**) of reovirus type 3 Dearing strain isolate R124 were obtained from the Nucleotide database of the National Center for Biotechnology Information (NCBI, Bethesda MD, USA) (20) and individually loaded into the NetMHC 4.0 Server. Peptide length was set at 8-11 amino acids and thresholds for predicted affinity were set at <0.5% (strong binders) and >2.0% (weak binders) for murine MHC-I molecule H-2K^b. Predicted peptides of all segments were combined and sorted on binding affinity (nM) and rank. Peptides (**Table S3**) with rank <0.200 were ordered as a micro-scale crude peptide library (GenScript, Leiden, The Netherlands) and their recognition by the reovirus-specific T-cell bulk was assessed using intracellular cytokine staining.

Intracellular cytokine staining

T cells from the reovirus-specific T-cell bulk or ex vivo tissues were co-cultured with reovirus-infected target cells (E/T = 1:1) or peptides (1 μg/mL). Unless otherwise indicated, the irrelevant cell line TC1 was used as target. Alternatively, serial dilutions of peptides ranging from 10 μM to 10 pM were added to T cells from the reovirus-specific T-cell bulk. When peptides were presented in the context of D1 cells,

peptides were incubated with D1 cells for one hour before overnight incubation with lipopolysaccharides (LPS, 10 ug/mL). For SLP processing experiments, D1 cells were pre-incubated for 1 hour with SLPs in concentrations between 10 µM and 1 pM after which lipopolysaccharide (LPS; 10 µg/mL) was added to each well for an additional 23 hours. Effector cells and target cells, peptides, or peptide-loaded D1 cells were co-cultured for 6 hours in the presence of BD GolgiPlug™ (BD Biosciences). PMA (20 ng/mL) and ionomycin (1 µg/mL) were used as a positive control. After incubation, cells were washed and stained for CD8α (53-6.7; BioLegend). Thereafter, cells were fixed with Fixation Buffer (BioLegend) according to the manufacturer's instructions, followed by staining for intracellular IFNγ (XMG1.2; BioLegend). After completion of the staining protocol, samples were fixed in 1% paraformaldehyde and acquired using a BD LSRFortessa™ X20 cell analyzer (BD Biosciences).

RNA isolation and RT-qPCR

A representative snap-frozen proportion (10-30 mg) of each tumor or organ was disrupted using a stain-less bead and the TissueLyser LT (Qiagen). Total RNA of *in vivo* samples was using the ReliaPrep™ RNA Tissue Miniprep System (Promega) according to the manufacturer's protocol. Reovirus genomic copies and expression levels of host genes (**Table S4**) in tumors were measured by RT-qPCR as previously described (11). Reovirus S4 copy numbers were determined based on a standard curve, generated with serial dilutions of plasmid pcDNA_S4. Log_{10} S4 copy numbers were calculated using a previously described formula (21). The expression of host genes was normalized to reference genes *Mzt2* and *Ptp4a2* using the Bio-Rad CFX Manager 3.1 Software (Bio-Rad).

Western blotting

Expression of reovirus µ1 protein in KPC3 tumors was analyzed by Western blotting. Briefly, snap-frozen KPC3 tumor pieces were lysed in radioimmunoprecipitation assay (RIPA) buffer containing protease and phosphatase inhibitors using a stain-less bead and the TissueLyser LT (Qiagen). Proteins (40 µg) were separated on a 4-15% mini-protean TGX gel (Bio-Rad) and then transferred to a 0.2 µM nitrocellulose membrane (Bio-Rad). After blocking for 1h at RT with Pierce™ Protein-Free (TBS) Blocking Buffer (ThermoFisher Scientific), the membrane was incubated overnight at 4°C with anti-µ1 (clone 10F6; Developmental Studies Hybridoma Bank, 1:200) or anti-β-actin (Cell Signaling Technology; 1:1000), followed by horseradish peroxidase (HRP)-conjugated goat anti-mouse IgG+IgM+IgA (Abcam, 1:1000) or HRP-conjugated goat anti-rabbit IgG (Cell Signaling Technology, 1:2000) at RT for 1 hour. Proteins were detected on the Chemidoc imaging XRS+ system (Bio-Rad) using the Clarity Western ECL Substrate kit (Bio-Rad).

Statistics

Group size was calculated using the PS: Power and Sample Size Calculation program (Vanderbilt University, version 3.1.6) (22). For experiments where tumor growth was the experimental read-out, mice were excluded when tumor engraftment was not successful (1% of all tumor engraftments). For RT-qPCR analysis, samples were excluded when

RNA concentration and purity were too low. For flow cytometry data, tumor samples were excluded when evidence for draining lymph node contamination was present. All graphs were prepared and statistical analyses were performed using the GraphPad Prism software (version 8.0.2). Statistical tests used for each figure are described in the figure legends. Experimental data were assumed to be normally distributed in all cases, except in the case of RT-qPCR data where standard deviations in Reo groups were significantly different compared to PBS groups. Significance levels are labeled with asterisks, with *p<0.05, **p<0.01, ***p<0.001, and ****p<0.0001. Non-significant differences are indicated by ns.

RESULTS

Identification of immunodominant reovirus CD8⁺ T-cell epitope

The use of oncolytic viruses is an attractive approach to increase $CD8^+$ T-cell influx in solid tumors with an immune-silent phenotype. Indeed, intratumoral injections with oncolytic reovirus in mice bearing murine pancreatic KPC3 tumors or epithelial lung TC1 tumors significantly enhance the frequency of $CD8^+$ T cells in these tumors (**Figure 1A-B, S1A,B**) (11). When these tumor-infiltrating lymphocytes (TILs) were examined for their specificity, we observed that TILs from reovirus-injected tumors only responded when the irrelevant, reovirus-infected TC1 cell line was used as a target (**Figure 1C, S1C**). This suggests that TILs of reovirus-treated mice were mainly reovirus-specific but not tumor-specific. To enable more detailed studies on the role of T cells during reovirus therapy, we set forth to identify the reovirus-derived epitopes recognized by the T cells. Since reovirus-specific T cells were also found in the spleen (**Figure 1C, S1C**), we utilized this splenic population of reovirus-specific $CD8^+$ T cells to generate a reovirus-specific T-cell bulk culture that could be used for epitope identification (**Figure 1D**). After a few rounds of in vitro restimulation with reovirus-infected target cells, a large proportion of the bulk recognized reovirus-infected target cells (**Figure 1E**). The response of reovirus-specific T-cell bulk was restricted by murine H-$2K^b$, as IFNγ was only produced in response to reovirus-infected Fisher rat embryo (FRE) FRE.K^b cells and not to infected FRE.D^b cells, even though infection efficiency was similar in both cell lines (**Figure 1F, S2A, B**).

Next, we determined the H-$2K^b$-specific reovirus-derived peptides that are recognized by reovirus-specific T cells. Predicted epitopes with a length between 8-11 amino acids from the sequences of all reovirus type 3 Dearing segments were divided into 10 pools and tested for their recognition by the reovirus-specific T-cell bulk using intracellular IFNγ staining (**Figure 1G, S3**). Peptide pools #2, #6, #7, and #9 were predominantly recognized. Therefore, peptides from these 4 pools were individually tested. Although some peptides such as peptides #29 and #42 induced IFNγ production, especially two length variant peptides #9 (*VSPKYSDL*) and #34 (*VSPKYSDLL*) activated a high percentage of T cells, comparable to the response against reovirus-infected target cells (**Figure**

1H). This indicated that these peptides might be recognized by the majority of T cells from the reovirus-specific T-cell bulk.

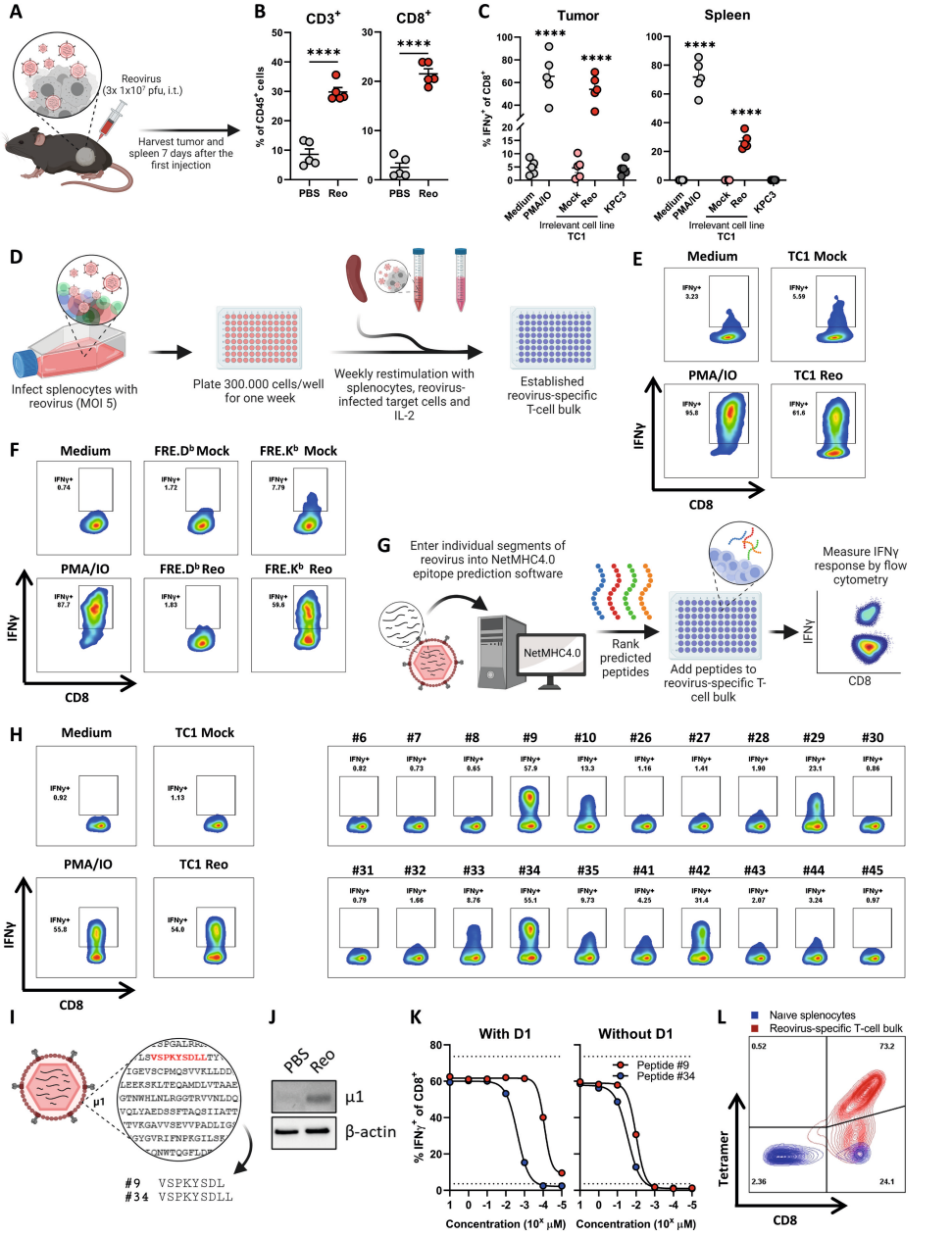

Figure 1. Identification of immunodominant reovirus CD8⁺ T-cell epitope. (**A**) Design of the experiment described in B-C. Mice (n=5/group) with established KPC3 tumors were intratumorally (i.t.) injected with reovirus (10^7 plaque-forming units (pfu)) on 3 consecutive days. Tumors and spleen were analyzed ex vivo 7 days after the first reovirus injection. (**B**) Frequency of CD3⁺ and CD8⁺ T cells within the total CD45⁺ immune cell population in KPC3 tumors after reovirus administration.

>>

>> (**C**) Frequency of interferon gamma (IFNγ)$^+$ cells within the intratumoral and splenic CD8$^+$ T-cell population as measured with intracellular cytokine staining. Single-cell suspensions (n=5/group) were cocultured with indicated targets. PMA/ionomycin (IO) was used as a positive control, and the irrelevant cell line TC1 was used as target cell line for reovirus infection. (**D**) Schematic overview of generation of reovirus-specific T-cell bulk. (**E, F**) Frequency of IFNγ$^+$ cells within reovirus-specific T-cell bulk after coculture with indicated targets. (**G**) Schematic overview of peptide prediction and testing. (**H**) Frequency of IFNγ$^+$ cells within reovirus-specific T-cell bulk after coculture with individual peptides from positive pools (Supplementary Figure S3). (**I**) Schematic overview of sequence and location of two dominant peptides. (J) Expression of reovirus μ1 protein in reovirus-treated KPC3 tumor. (**K**) Frequency of IFNγ$^+$ cells within reovirus-specific T cell bulk after coculture with titrated amounts of peptide #9 or #34. Peptides were added directly or pre-loaded for 1 hour on LPS-matured D1 dendritic cells. (**L**) Binding of generated H-2K^b-*VSPKYSDL* (Reo μ1$_{133\text{-}140}$)-tetramer to naive splenocytes or reovirus-specific T-cell bulk, as measured with flow cytometry. Data are presented as mean±SEM. Statistical tests used: (B): unpaired t-test between PBS and Reo groups. (C): ordinary one-way analysis of variance (ANOVA) with Dunnett's post hoc test. Statistical difference was compared to medium control group. Significance level: ****p<0.0001.

Peptides #9 and #34 are derived from the reovirus outer-capsid protein μ1, a protein that is expressed in reovirus-treated tumors (**Figure 1I, J**). Peptide #9 was found in H-2K^b on the surface of reovirus-infected cells in another study, indicating that this peptide can be processed and presented (23). Subsequently, peptides #9 and #34 were titrated and co-cultured with reovirus-specific T cells, either added directly or in the presence of professional antigen-presenting cells (**Figure 1K**). This showed that the T cells responded to lower concentrations of peptide #9 when compared to peptide #34 and, therefore, peptide #9 (named Reo μ1$_{133\text{-}140}$)was used to generate a reovirus-specific H-2K^b-tetramer. This tetramer did specifically bind to T cells from the reovirus-specific T-cell bulk and not to naive splenocytes (**Figure 1L**), indicating that this tetramer allows selective staining of reovirus-specific T cells.

Intratumoral delivery of reovirus induces a systemic reovirus-specific T-cell response that is enriched in the tumor

We used this Reo μ1$_{133\text{-}140}$tetramer (Tm) to interrogate reovirus-specific T-cell immunity in the blood of KPC3 tumor-bearing mice after intratumoral administration of reovirus (**Figure 2A**). We observed a reovirus-specific, Tm$^+$ CD8$^+$ T-cell population 5 days after the first intratumoral injection (**Figure 2B**), the frequency of which peaked at day 7 with percentages ranging from 1.7% to 12.8% Tm$^+$ cells out of all CD8$^+$ T cells. Next, we examined the location and frequency of reovirus-specific T cells in the spleen, tumor-draining lymph node (TDLN), and tumor 7 days after intratumoral reovirus administration. Reovirus-specific T cells were found in small frequencies in the TDLN, in the spleen, and at high frequencies in the tumor (**Figure 2C, D**). A similar distribution of Tm$^+$ CD8$^+$ T cells over the lymphoid organs and tumors was observed in TC1 tumor-bearing mice after intratumoral injection with reovirus (**Figure S4**). Tm$^+$ CD8$^+$ T cells were also present in tumors of mice that were injected with Jin-3 (12,24), a variant of the reovirus Type 3 Dearing strain with enhanced tropism (**Figure S5**). These data suggest that the reovirus epitope is conserved among virus isolates and in different tumor models. Interestingly, the frequencies of Tm$^+$ CD8$^+$ T cells in blood, spleen, and

TDLN dropped drastically on day 12 after intratumoral reovirus administration but were retained at relatively high levels in the tumor (**Figure 2E**).

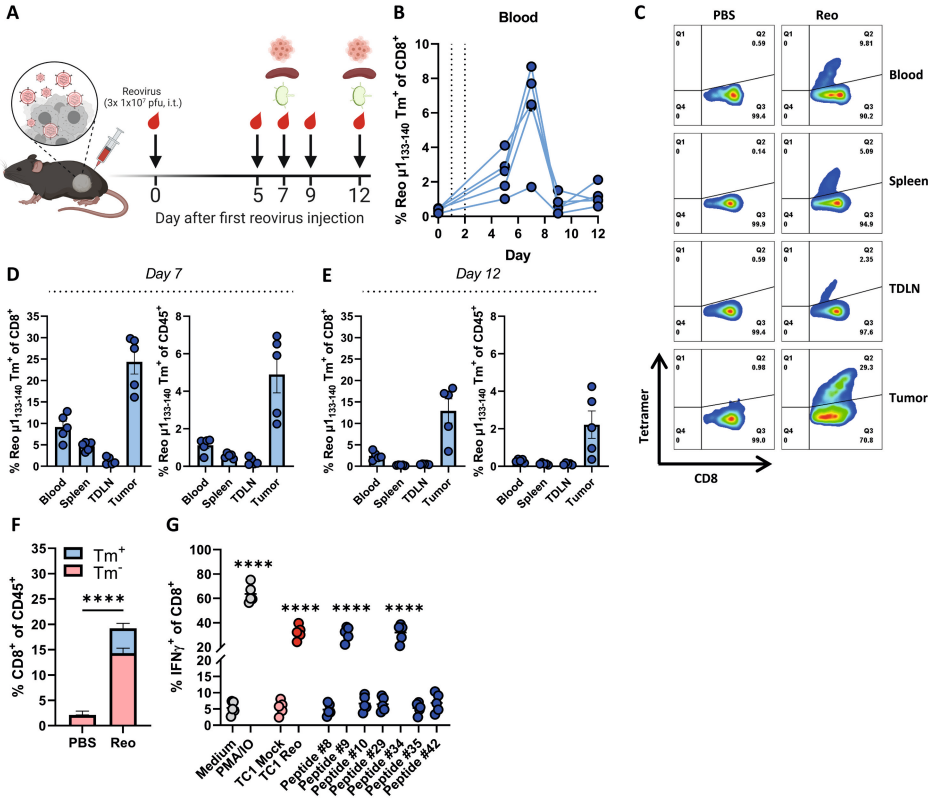

Figure 2. Intratumoral delivery of reovirus induces a systemic reovirus-specific T-cell response that is enriched in the tumor. (**A**) Design of the experiment described in B-D. Mice (n=5/group) with established KPC3 tumors were intratumorally (i.t.) injected with reovirus (10^7 plaque-forming units (pfu)) on 3 consecutive days. Blood, tumors, spleens, and tumor-draining lymph nodes (TDLN) were analyzed using flow cytometry on indicated days. (**B**) Frequency of Reo $\mu1_{133\text{-}140}$ tetramer $(Tm)^+$ $CD8^+$ T cells in the blood on indicated days after intratumoral reovirus administration. (**C**) Representative flow cytometry plots of Tm^+ $CD8^+$ T cells in indicated organs on day 7 after the first reovirus injection. (**D, E**) Quantification of Tm^+ cells out of $CD8^+$ T cells and total $CD45^+$ immune cell population in indicated organs. (**F**) Separation of Tm^+ cells from Tm^- cells within the total $CD8^+$ T cell population of reovirus-treated KPC3 tumors. (**G**) Frequency of interferon gamma $(IFN\gamma)^+$ cells within the intratumoral $CD8^+$ T-cell population after coculture with indicated targets as measured with intracellular cytokine staining. PMA/ionomycin (IO) was used as a positive control. All data are presented as mean±SEM. Statistical tests used: (F): unpaired t-test between PBS and Reo group. (G): ordinary one-way analysis of variance (ANOVA) with Dunnett's post hoc test. Statistical difference was compared to medium control group. Significance level: ****$p<0.0001$.

Whilst a substantial population within $CD8^+$ TILs was Tm^+, there was also a Tm^- $CD8^+$ T-cell fraction (**Figure 2F**). We already demonstrated that this Tm^- fraction was not tumor-specific (**Figure 1, Figure S1**), suggesting that reovirus administration either led to the influx of bystander T cells or reovirus-specific T cells directed to another reovirus-derived epitope. To test this, TILs from reovirus-treated mice were co-cultured with the other peptides that were also recognized by the splenocyte-derived reovirus-specific T-cell bulk (**Figure 1H**). However, none of these peptides elicited a detectable response in the TILs (**Figure 2G**). This suggests that a large majority of the reovirus-specific T-cell response is directed against an immunodominant $CD8^+$ T-cell epitope, similar to what is observed for LCMV (25), influenza (26), and the oncolytic vesicular stomatitis virus (VSV) (27).

cDC1s are involved in the priming of reovirus-specific T cells

Because intratumoral administration of reovirus also resulted in high numbers of systemic reovirus-specific T cells, we were interested in which cell types are involved in the priming of these reovirus-specific T cells. Within the family of antigen-presenting cells, the low-frequent population of basic leucine zipper transcriptional factor ATF-like 3 (*Batf3*)-driven cross-presenting dendritic cells (cDC1) are highly specialized in shaping $CD8^+$ T-cell responses through uptake and processing of exogenous antigens for their presentation in the context of MHC-I molecules, including viral antigens (28-32). Therefore, we studied reovirus-specific immunity in *Batf3*$^{-/-}$ mice, which contained significantly decreased numbers of cDC1 in the spleen and peripheral organs (**Figure S6A, B**) (32,33). Both wild-type C57BL/6J and *Batf3*$^{-/-}$ mice were engrafted with a KPC3 tumor and received intratumoral reovirus injections (**Figure 3A**). An in-depth analysis of the tumor immune cell infiltrate revealed that the total $CD45^+$ immune cell population (**Figure 3B**) or the reovirus-induced influx of NK (**Figure 3C**) and $CD4^+$ T cells (**Figure 3D**) was not affected by *Batf3*-deficiency. However, the influx of total $CD8^+$ T cells was significantly decreased in reovirus-treated *Batf3*$^{-/-}$ mice (**Figure 3E**). This lower $CD8^+$ T-cell influx probably reflects the impaired systemic priming of reovirus-specific $CD8^+$ T cells, since *Batf3*$^{-/-}$ mice displayed significantly lower frequencies of reovirus-specific $CD8^+$ T cells in the tumor, as well as in the blood, spleen, and TDLN (**Figure 3E**). The attraction of $CD8^+$ T cells to the tumor was most likely not the limiting factor in *Batf3*$^{-/-}$ mice since reovirus replication and the reovirus-induced expression of ISGs, including the T-cell attracting chemokines *Cxcl9* and *Cxcl10*, were not affected (**Figure 3F, G**). Combined, these data indicate that cDC1s play an important role in the priming of reovirus-specific T cells.

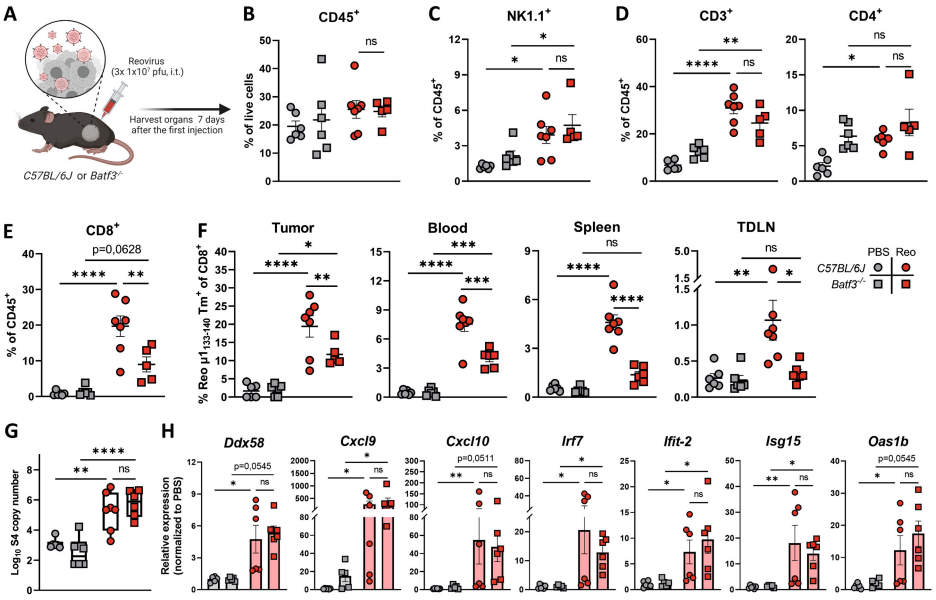

Figure 3. cDC1s are involved in priming of reovirus-specific T cells. (**A**) Design of the experiment described in (B-H). *C57BL/6J* or *Batf3*$^{-/-}$ mice (n=5–7/group) with established KPC3 tumors were intratumorally (i.t.) injected with reovirus (10^7 plaque-forming units (pfu)) on 3 consecutive days. Blood, tumors, spleens, and tumor-draining lymph nodes (TDLN) were analyzed 7 days after the first reovirus injection using flow cytometry. (**B**) Total CD45$^+$ immune cell population in KPC3 tumors of *C57BL/6J* or *Batf3*$^{-/-}$ mice after reovirus administration. (**C**) Intratumoral frequency of NK1.1$^+$ cells within CD45$^+$ immune cells. (**D**) Intratumoral frequency of CD3$^+$ and CD4$^+$ T cells within CD45$^+$ immune cells. (**E**) Intratumoral frequency of CD8$^+$ T cells within CD45$^+$ immune cells. (**F**) Frequency of Reo $\mu1_{133\text{-}140}$ tetramer (Tm)$^+$ CD8$^+$ T cells in indicated organs after intratumoral reovirus administration. (**G**) Intratumoral presence of reovirus genomic segment 4 (S4) copy numbers as measured by quantitative reverse transcription PCR (RT-qPCR). (**H**) Relative expression of various interferon response genes as determined by RT-qPCR. All data are presented as mean±SEM. One tumor of the *Batf3*$^{-/-}$ Reo group in figures B-E was excluded due to lymph node contamination. Statistical tests used: (B-G): ordinary one-way analysis of variance (ANOVA) with Tukey's post hoc test. (H): Nonparametric Kruskal-Wallis test with Dunn's multiple comparisons test. Significance levels: *p<0.05, **p<0.01, ***p<0.001, and ****p<0.0001.

Tumor-infiltrated reovirus-specific T cells have a pronounced effector phenotype

Next, we assessed the phenotype of Reo $\mu1_{133\text{-}140}$-specific CD8$^+$ T cells (Tm$^+$) and investigated whether their phenotype is influenced by their location. Tm$^+$ CD8$^+$ T-cell populations from blood, spleen, TDLN, and tumor were analyzed with OMIQ analysis software that clustered cells based on their expression of CD44, CD62L, KLRG1, CD69, PD1, and Tim3. The tumor-residing Tm$^+$ CD8$^+$ T cells clustered separately from Tm$^+$ CD8$^+$ T cells found in other organs (**Figure 4A**). Tumor-residing Tm$^+$ CD8$^+$ T cells had a higher expression of activation markers CD69, PD1, and Tim3 compared to Tm$^+$ CD8$^+$ T cells in other organs (**Figure 4B**). This suggests that reovirus-specific TILs obtain a unique and distinct phenotype upon reaching the tumor, most likely because this is where reovirus is replicating and the reovirus epitope is presented (**Figure 1J**).

When the same analysis was applied to tetramer-negative $CD8^+$ T cells (**Figure 4C**), we observed a cluster within this population with a similar phenotype as Tm^+ $CD8^+$ T cells, with high expression of CD69, PD1, and Tim3 (**Figure 4D**). These Tm^- $CD8^+$ T cells may also be reovirus-specific, but recognize other, yet unidentified reovirus-derived epitopes. The other intratumoral Tm^- $CD8^+$ T cell cluster, with low expression of CD69, PD1, and Tim3 overlaps with $CD8^+$ T cells that are found in the blood and the spleen, suggesting that this population encompasses mainly 'bystander' $CD8^+$ T cells.

Direct comparison and quantification of expression profiles of Tm^+ and Tm^- $CD8^+$ T cells revealed that in all indicated organs, Tm^+ $CD8^+$ T cells have a significantly more activated phenotype compared to Tm^- $CD8^+$ T cells (**Figure 4E**). This effector phenotype of Tm^+ $CD8^+$ T cells remained stable until 12 days after intratumoral reovirus administration (**Figure S7**). Collectively, these data show that reovirus-specific T cells are highly activated and demonstrate a pronounced effector phenotype when present in the tumor, which distinguishes them from 'bystander' $CD8^+$ T cells. Targeting these reovirus-specific T cells might therefore be an attractive solution for low-immunogenic tumors where tumor-specific T cells are absent.

Route of reovirus administration impacts intratumoral influx, but not priming of reovirus-specific T cells

We next investigated whether intravenous administration of reovirus, which is the route applied in the clinic, also recruits antigen-specific T cells to the tumor. Therefore, the frequency and location of reovirus-specific $CD8^+$ T cells were compared between intravenous and intratumoral administration of reovirus (**Figure 5A**). Interestingly, both intravenous, as well as intratumoral reovirus administration in tumor-bearing mice resulted in similar systemic frequencies of reovirus-specific T cells, suggesting effective systemic priming occurs independently of the reovirus administration route (**Figure 5B**). Surprisingly, equal levels of reovirus-specific T cells were also found in mice without a tumor, demonstrating that active reovirus replication in the tumor is not essential for the priming of a potent systemic reovirus-specific T-cell response (**Figure 5B**).

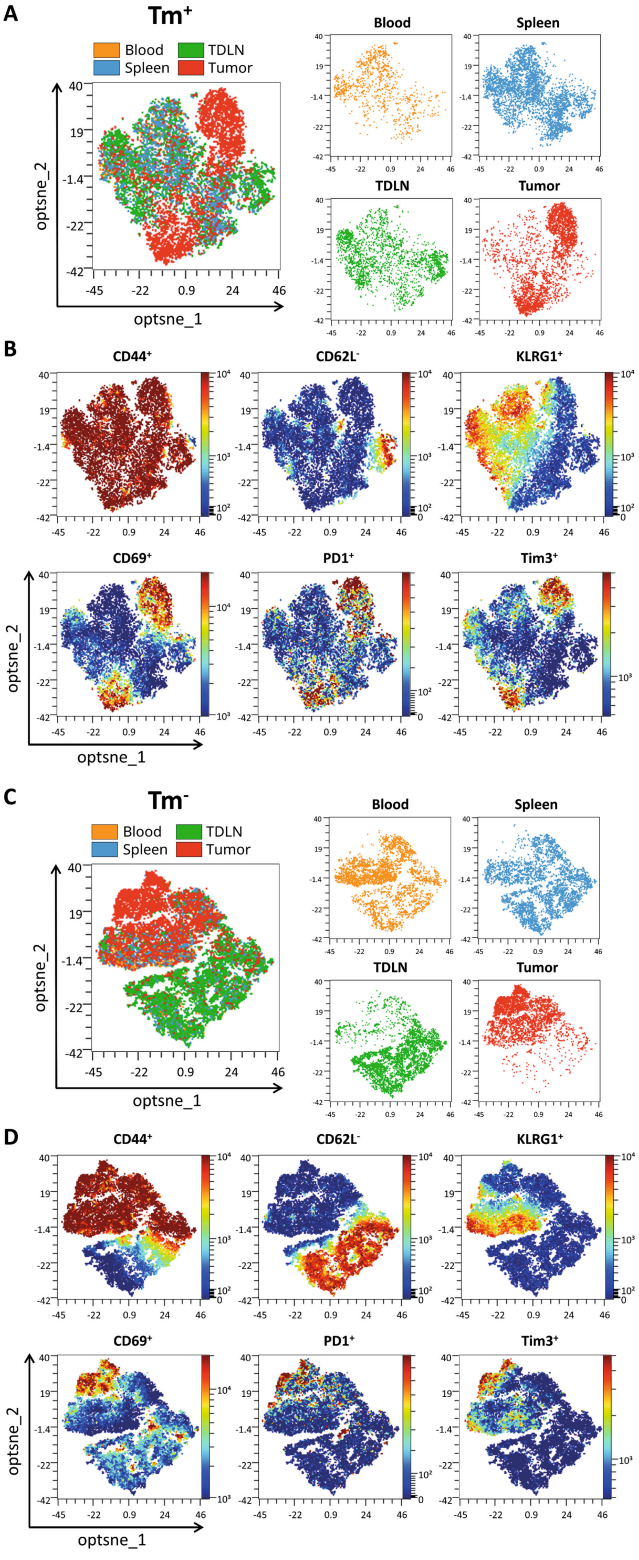
A
Tm+
Blood
Spleen
TDLN
Tumor
optsne_2
optsne_1
B
CD44+
CD62L-
KLRG1+
CD69+
PD1+
Tim3+
C
Tm-
D

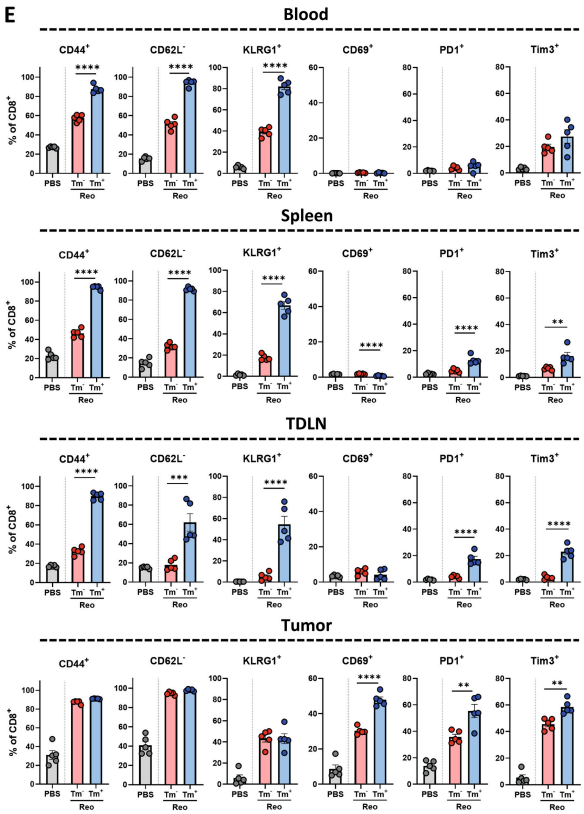

Figure 4. Tumor-infiltrated reovirus-specific T cells have a potent effector phenotype. (**A/C**) Opt-SNE cluster plots of Reo $\mu1_{133-140}$ tetramer $(Tm)^+$ (A) or Tm^- (C) $CD8^+$ T cells from indicated organs. 1000 Tm^+ $CD8^+$ T cells or the maximum possible number of cells if Tm^+ $CD8^+$ T cells <1000 were subsampled from individual organs of each mouse. (**B/D**) Expression intensity profile of activation markers on Tm^+ (B) or Tm^- (D) $CD8^+$ T cells. (**E**) Quantification of expression of activation markers on Tm^- or Tm^+ $CD8^+$ T cells in the blood, spleen, tumor-draining lymph node (TDLN), or tumor (n=5/group) of mice treated with Reo, compared to untreated (PBS). Samples were harvested 7 days after the first intratumoral reovirus injection and the expression of indicated markers was measured using flow cytometry. All data are presented as mean±SEM. Statistical tests used: (E): ordinary one-way analysis of variance (ANOVA) with Tukey's post hoc test. Significance levels: *p<0.05, **p<0.01, ***p<0.001, and ****p<0.0001.

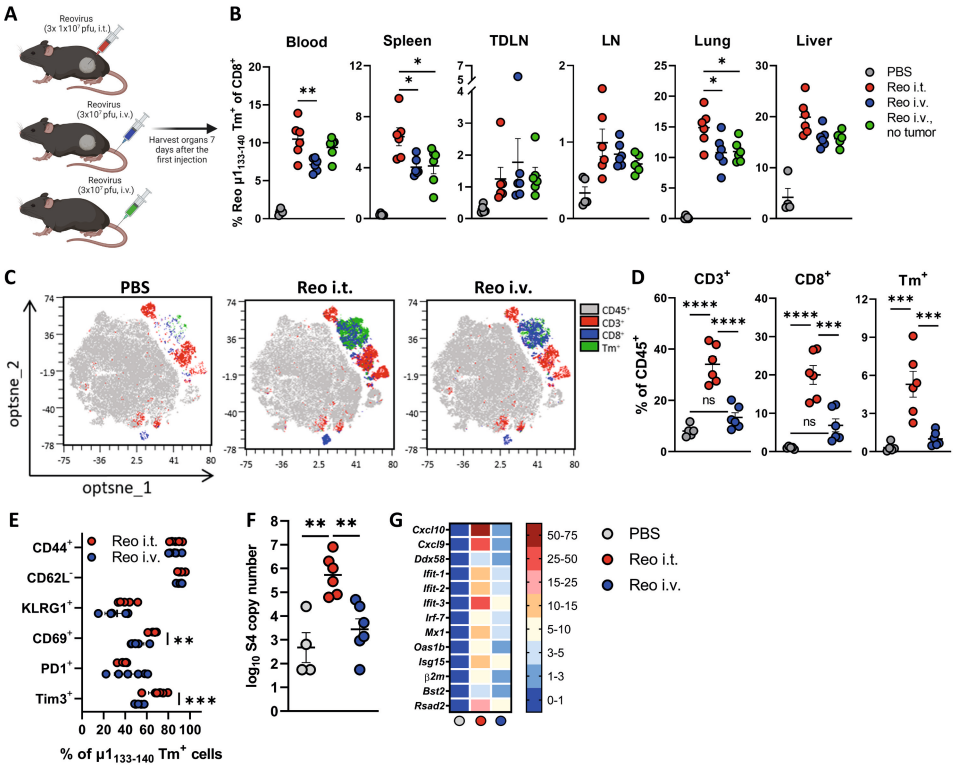

Figure 5. Route of reovirus administration impacts intratumoral influx, but not priming of reovirus-specific T cells. (**A**) Schematic overview of reovirus administration routes, in mice with or without a tumor. (**B**) Frequency of Reo $\mu1_{133\text{-}140}$ Tm^+ $CD8^+$ T cells in indicated organs 7 days after reovirus administration. (**C**) Opt-SNE plots highlighting the intratumoral presence of $CD3^+$, $CD8^+$, and Tm^+ T cells after indicated treatments. 10.000 $CD45^+$ cells were subsampled from each sample or the maximum possible number of cells if $CD45^+$ cells <10000. (**D**) Intratumoral frequency of $CD3^+$, $CD8^+$, and Tm^+ T cells within $CD45^+$ immune cells after indicated treatments. (**E**) Expression of activation markers on Tm^+ $CD8^+$ T cells in the tumor after intratumoral or intravenous reovirus administration. (**F**) Intratumoral presence of reovirus genomic segment 4 (S4) copy numbers as measured by quantitative reverse transcription PCR (RT-qPCR). (**G**) Heatmap depicting relative expression of various interferon response genes as determined by RT-qPCR. Data are presented as mean±SEM. Statistical tests used: (B, D, F): ordinary one-way analysis of variance (ANOVA) with Tukey's post hoc test. (E): ordinary two-way ANOVA with Sidak's post hoc test. Significance levels: *p<0.05, **p<0.01, ***p<0.001, and ****p<0.0001.

Although systemic priming of reovirus-specific $CD8^+$ T cells was equally effective, we observed that the reovirus-induced influx of (reovirus-specific) $CD8^+$ T cells was severely impaired in tumors of mice that received reovirus intravenously, although a small population of T cells could still be observed (**Figure 5C, D**). Additionally, while the expression levels of CD44, CD62L, KLRG1, and PD1 on the few intratumoral Tm^+ $CD8^+$ T cells after intravenous reovirus administration were relatively similar to the Tm^+ $CD8^+$ T cells that were present after intratumoral reovirus administration, their expression of CD69 and Tim3 was significantly lower (**Figure 5E**). The number of reovirus genomic copies (**Figure 5F**) and the reovirus-induced expression of ISGs (**Figure 5G**) in the tumor was also significantly lower in mice that received intravenous administration of reovirus, suggesting that T-cell influx is connected with either reovirus replication or reovirus-induced expression of ISGs or a combination of both. In conclusion, these data indicate that systemic frequency and location of reovirus-specific $CD8^+$ T cells are not influenced by the route of reovirus administration, but that intratumoral reovirus administration is preferred to induce higher densities of these reovirus-specific $CD8^+$ T cells in the tumor.

Reovirus-specific T cells are amenable to peptide-mediated reactivation

We next asked if the limited influx of reovirus-specific T cells in the tumor upon intravenous reovirus administration could be enhanced by local repeated T-cell receptor (TCR)-triggering. To uncouple reactivation and expansion of reovirus-specific T cells from other reovirus-mediated effects, we intratumorally injected the reovirus-derived Reo $\mu1_{133\text{-}140}$ peptide (*VSPKYSDL*) instead of replicating reovirus (**Figure 6A**). Injection of Reo $\mu1_{133\text{-}140}$ peptide in the tumor after intravenous reovirus administration significantly enhanced the percentage of intratumoral (reovirus-specific) T cells similar to that observed when reovirus was intratumorally administered (**Figure 6B**). Within the intratumoral and splenic $CD8^+$ T-cell populations, the frequency of reovirus-specific T cells was significantly increased when Reo $\mu1_{133\text{-}140}$ peptide was injected, suggesting that reactivation of reovirus-specific T cells led to specific expansion of this population (**Figure 6C**). The additional administration of peptide Reo $\mu1_{133\text{-}140}$ also specifically enhanced the effector phenotype of reovirus-specific T cells, as demonstrated by high CD44, PD1, and Tim3 expression in the tumor and the spleen (**Figure 6D**), implying that T cells induced by intravenously applied reovirus can be turned into fully activated effector cells with a phenotype comparable to those generated via intratumoral application.

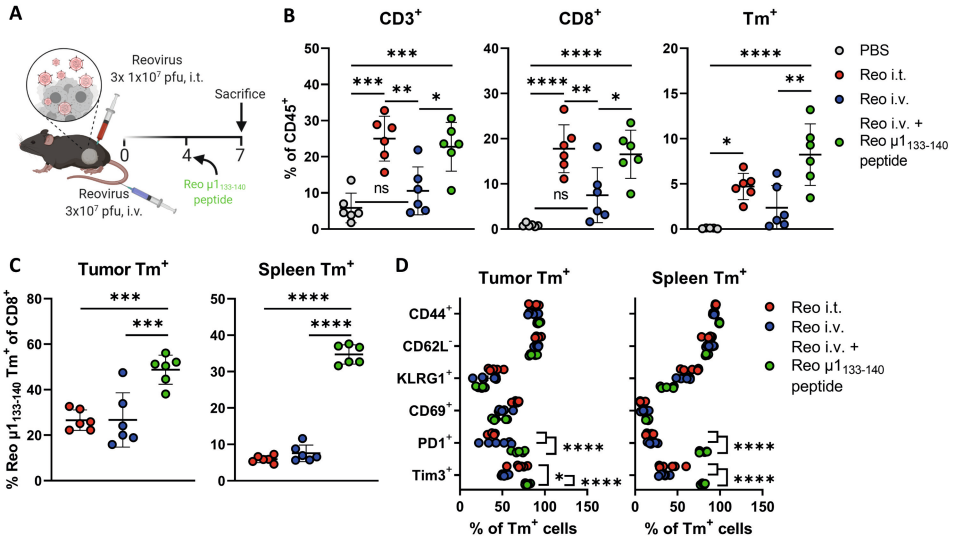

Figure 6. Reovirus-specific T cells are amenable to peptide-mediated reactivation. (**A**) Design of the experiment described in (B-E). Mice (n=6/group) with established KPC3 tumors were intratumorally (i.t.) injected with reovirus (10^7 plaque-forming units (pfu)) on days 0, 1, and 2, or intravenously (i.t.) injected on day 0 with $3x10^7$ pfu of reovirus. One group of mice that received reovirus i.v. additionally received an i.t. injection with the Reo $\mu1_{133-140}$ peptide (50 μg) on day 4, after which mice were sacrificed on day 7 for ex vivo analysis. (**B**) Intratumoral frequency of $CD3^+$, $CD8^+$ and Tm^+ T cells within the $CD45^+$ population. (**C**) Frequency of Reo $\mu1_{133-140}$ Tm^+ $CD8^+$ T cells out of $CD8^+$ T cell population in tumor and spleen. (**D**) Expression of activation markers on Tm^+ $CD8^+$ T cells in the tumor and spleen after indicated treatments. All data are presented as mean±SEM. Statistical tests used: (B-C): ordinary one-way analysis of variance (ANOVA) with Tukey's post hoc test. (D) ordinary two-way ANOVA with Tukey's post hoc test. Significance levels: *p<0.05, **p<0.01, ***p<0.001, and ****p<0.0001.

Induction of vaccine-induced reovirus-specific T-cell immunity enhances the anticancer efficacy of reovirus therapy

We showed that reovirus-specific T cells are potent effector cells that are present in the tumor, which makes them very attractive to use as anticancer effector cells, especially when tumor-specific T cells are unavailable. We hypothesized that these reovirus-specific T cells, when available in sufficiently high numbers, would be able to kill virus-infected cells in the tumor microenvironment that display viral epitopes on their cell surface. To optimally stimulate the frequency of this reovirus-specific T-cell population, we developed a vaccination strategy to install a preexisting pool of circulating reovirus-specific T cells before tumor inoculation. We designed a synthetic long peptide (SLP) that was derived from the natural sequence of the reovirus μ1 protein and contains the immunodominant Reo $\mu1_{133-140}$ epitope of reovirus. *In vitro*, the SLP was processed and presented efficiently by murine dendritic D1 cells and was able to induce activation of T cells from the reovirus-specific T-cell bulk (**Figure S8**). Next, we vaccinated naive mice with the SLP, using a prime-boost schedule (**Figure 7A**) that induced high frequencies of Tm^+ $CD8^+$ T cells in the circulation (**Figure 7B**). These circulating Tm^+ $CD8^+$ T cells displayed a potent effector phenotype as evidenced by their expression of activation markers CD44, KLRG1, PD1, and Tim3 (**Figure 7C**).

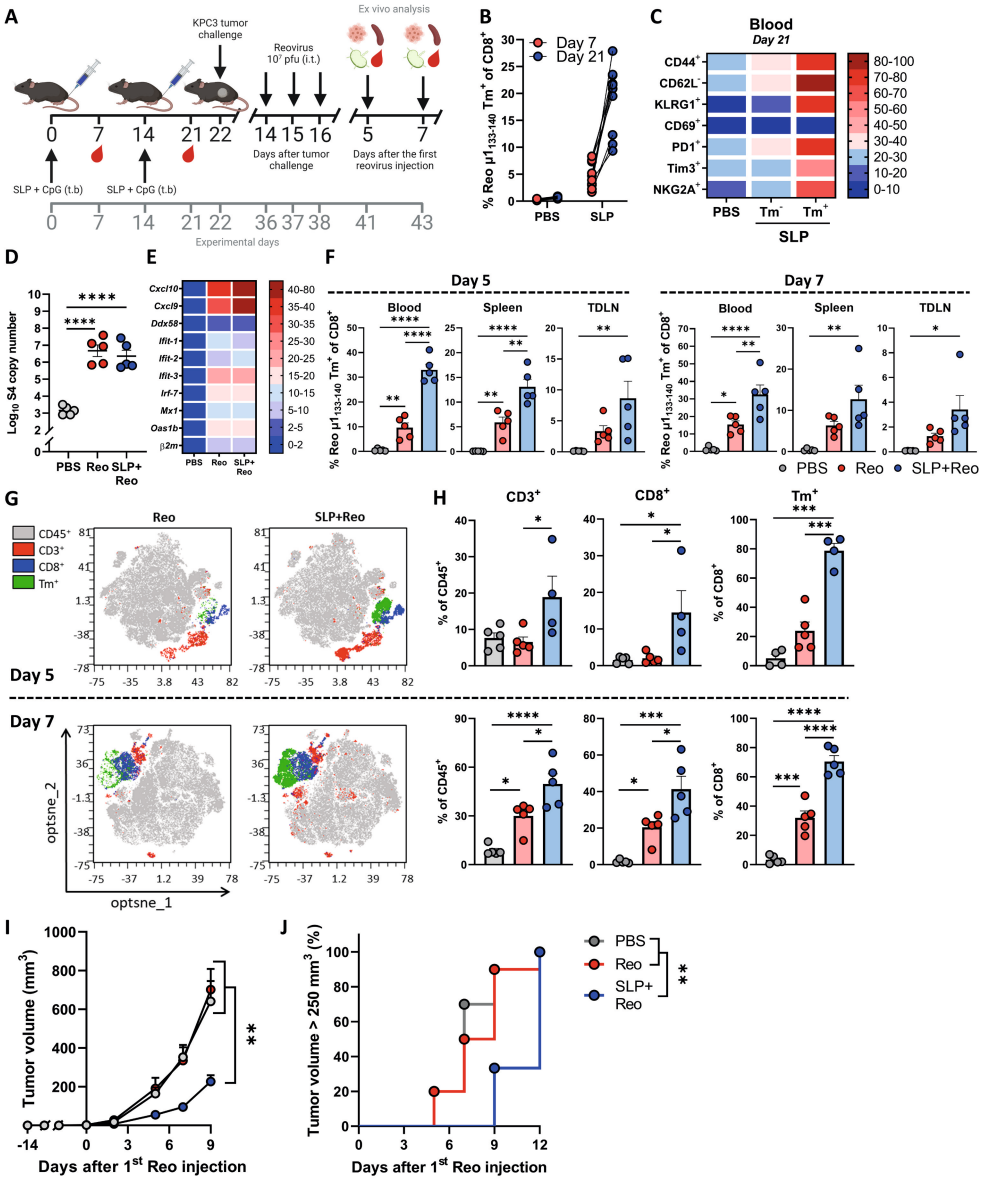

Figure 7. Induction of vaccine-induced reovirus-specific T-cell immunity enhances the anticancer efficacy of reovirus therapy. (**A**) Design of the experiment described in (B-H). Naive mice (n=10/group) were vaccinated on days 0 and 14 by injecting 100 μg SLP together with 20 μg CpG in the tail-base region. On day 22, KPC3 tumor challenge was performed. Mice with established KPC3 tumors were intratumorally (i.t.) injected with reovirus (10^7 plaque-forming units (pfu)) on days 14, 15, and 16 after the tumor challenge. Mice were sacrificed on day 5 (n=5/group) and 7 (n=5/group) after the first i.t. reovirus injection for ex vivo analysis. (**B**) Frequency of Reo $\mu1_{133-140}$ Tm^+ cells within $CD8^+$ T cells 7 days after priming vaccination and 7 days after boosting vaccination. (**C**) Heatmap showing activation profile of Tm^+ $CD8^+$ T cells in blood on day 21. (**D**) Intratumoral presence of reovirus genomic segment 4 (S4) copy numbers on day 5 after the first reovirus injection, as measured by quantitative reverse transcription PCR (RT-qPCR). (**E**) Heatmap depicting relative expression of various interferon response genes on day 5, as determined by RT-qPCR. >>

>> (**F**) Frequency of Tm^+ cells within $CD8^+$ T cells in blood, spleen, and tumor-draining lymph node (TDLN), 5 and 7 days after reovirus treatment. (**G**) Opt-SNE plots highlighting the intratumoral presence of $CD3^+$, $CD8^+$, and Tm^+ T cells after indicated treatments, on days 5 and 7. 10000 $CD45^+$ cells were subsampled from each sample or the maximum possible number of cells if $CD45^+$ cells <10000. (**H**) Intratumoral frequency of $CD3^+$, $CD8^+$, and Tm^+ T cells within $CD45^+$ immune cells on days 5 and 7. (**I**) Average growth curves of mice (n=9-10/group) receiving indicated treatments. (**J**) Kaplan-Meier graph showing accumulation of animals reaching tumor size > 250 mm^3. All data are presented as mean±SEM. One tumor of SLP+Reo Day 5 group in figure H was excluded due to lymph node contamination. One mouse of SLP+Reo group in figures I and J was excluded due to unsuccessful tumor engraftment. Statistical tests used: (D, F, H): ordinary one-way analysis of variance (ANOVA) with Tukey's post hoc test. (I): ordinary two-way ANOVA with Tukey's post hoc test. (J): Mantel-Cox Log-rank test. Significance levels: *p<0.05, **p<0.01, ***p<0.001, and ****p<0.0001.

Vaccinated mice were subsequently implanted with a KPC3 tumor and palpable tumors were injected intratumorally on 3 consecutive days with reovirus. Notably, the preexisting presence of reovirus-specific T cells did not affect reovirus replication (**Figure 7D**) or reovirus-induced expression of ISGs in the tumor (**Figure 7E**). We next assessed frequencies of reovirus-specific $CD8^+$ T cells on days 5 and 7 after the first intratumoral reovirus injection. The presence of a vaccine-induced, reovirus-specific T-cell response significantly increased the frequency of reovirus-specific T cells in the blood, spleen, and TDLN upon intratumoral reovirus administration (**Figure 7F**). As expected, boosting of the preexisting reovirus-specific T-cell response by intratumoral reovirus administration mediated an earlier and higher intratumoral influx of $CD8^+$ T cells (SLP+Reo) than when this response had to be kick-started by intratumoral reovirus (Reo) administration (**Figure 7G, H**). In particular, the specificity of the intratumoral $CD8^+$ T-cell population was highly enriched for reovirus when mice were first primed by SLP vaccination. Around 75% of intratumoral $CD8^+$ T cells were reovirus-specific in the SLP+Reo group compared to an average of 25% in the Reo only group (**Figure 7G, H**).

This also resulted in a stronger antitumor effect. While intratumoral reovirus administration monotherapy does not affect tumor growth at the used dosage, a significant delay in tumor growth was observed when mice were vaccinated before intratumoral reovirus treatment, resulting in smaller tumors at later time points (**Figure 7I, J**). The enhanced antitumor effect was mediated by $CD8^+$ T cells since the SLP+Reo-induced antitumor effect was significantly decreased when CD8 T cells were depleted after vaccination (**Figure S9A-D**). Within the CD8 T-cell population, the reovirus-specific T cells were specifically responsible since vaccination with an irrelevant SLP vaccine targeting the HPV16 $E7_{49-57}$ epitope did not enhance the antitumor effect of Reo monotherapy (**Figure S10A-C**).

Although SLP+Reo delayed tumor outgrowth, tumors eventually reached the experimental endpoint. When we assessed these end-stage tumors for the presence of T cells, we observed that there was still a large population of reovirus-specific T cells present (**Figure S11A, B**). We investigated whether these T cells could be reinvigorated by combining SLP+Reo therapy with checkpoint blockade (αPD-L1), to possibly prolong

the delay in tumor growth. However, the addition of αPD-L1 did not enhance the efficacy of SLP+Reo therapy (**Figure S12A-C**). We next investigated whether we could enhance the antitumor effect of SLP+Reo therapy by additional reovirus administrations. Surprisingly, the continued intratumoral administration of reovirus also did not improve the antitumor effect of SLP+Reo therapy (**Figure S13A-C**). These observations suggest that there is a maximum level of control that reovirus-specific T cells can exert on the growth of the tumor.

Therapeutic boosting of a reovirus-induced, preexisting T-cell pool delays tumor growth

Lastly, we investigated whether SLP+Reo therapy can also be applied in a more therapeutically relevant setting. Since a large majority of the human population has encountered reovirus before, most cancer patients will have circulating reovirus-specific T cells. We investigated whether this preexisting reovirus-induced T-cell pool might also be exploited to improve the efficacy of reovirus therapy. Additionally, we investigated whether the SLP vaccine is still effective when applied in mice that already have a tumor. We immunized mice with live reovirus to induce preexisting immunity, and subsequently boosted the immunization-induced reovirus-specific T-cell response with the SLP, either before (BT – before tumor) or after (AT – after tumor) tumor inoculation (**Figure 8A**). In both immunized groups, reovirus-specific T-cell responses in the blood could be boosted to similar levels compared to naive mice that were vaccinated according to the prime-boost schedule, even when mice received the SLP after tumor inoculation, thus in a therapeutic setting (**Figure 8B**). No toxicity through changes in body weight could be observed (**Figure S14**), but tumor growth was significantly delayed in both immunized groups. This suggests that boosting the reovirus-specific T-cell response with an SLP in humans with preexisting immunity might also be safe and effective to enhance the efficacy of reovirus monotherapy (**Figure 8C, D**).

Taken together, we showed proof-of-concept data that high intratumoral frequencies of preinduced reovirus-specific T cells can be exploited to effectively impact tumor growth upon reovirus treatment, thereby circumventing the need for tumor-specific T cells. These data advocate for the use of vaccines aimed at inducing strong OV-specific T-cell responses to enhance the efficacy of OV monotherapy in tumors with low immunogenicity.

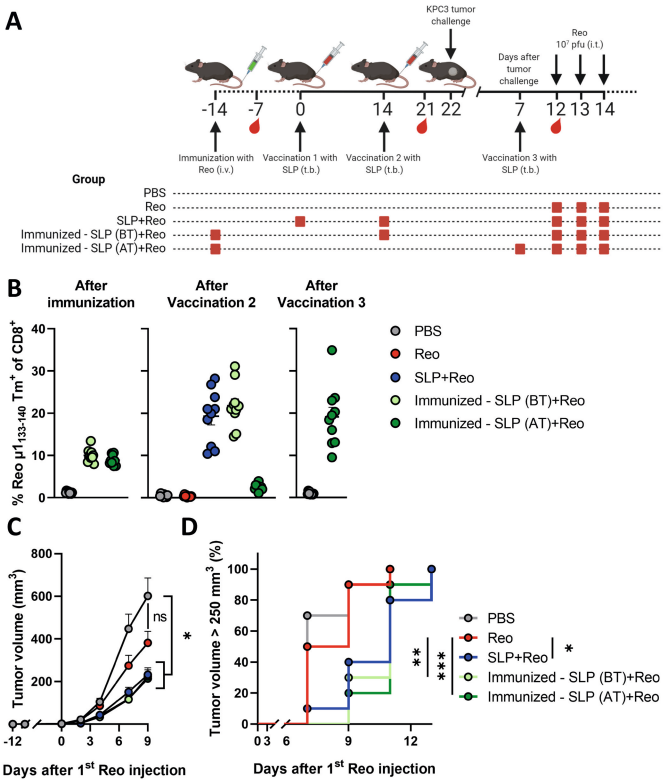

Figure 8. Therapeutic boosting of a reovirus-induced, preexisting T-cell pool delays tumor growth. (**A**) Design of the experiment described in (B-D). Naive mice (n=10/group) were immunized on day -14 by injecting reovirus (10^7 plaque-forming units (pfu)). Vaccination occurred on days 0 and/or 14 by injecting 100 µg SLP together with 20 µg CpG in the tail-base region. On day 22, KPC3 tumor challenge was performed. One group was vaccinated with the SLP on day 7 after tumor challenge. Intratumoral administration with reovirus (10^7 pfu) occurred on days 12, 13, and 14 after the tumor challenge. (**B**) Frequency of Reo $\mu1_{133\text{-}140}$ Tm^+ cells within $CD8^+$ T cells after immunization or vaccination. (**C**) Average growth curves of mice (n=10/group) receiving indicated treatments. (**D**) Kaplan-Meier graph showing accumulation of animals reaching tumor size > 250 mm^3. All data are presented as mean±SEM. Statistical tests used: (C): ordinary two-way ANOVA with Tukey's post hoc test. (D): Mantel-Cox Log-rank test. Significance levels: *p<0.05, **p<0.01, and ***p<0.001.

DISCUSSION

The mammalian reovirus type 3 Dearing strain (T3D), clinically known as Pelareorep, is one of the leading oncolytic viruses (OVs) under clinical evaluation (34). As monotherapy, reovirus has undergone clinical evaluation in trials across a range of indications, most of which have employed intravenous administration of reovirus. As recently reviewed by Müller et al, the clinical efficacy of reovirus as monotherapy has been modest (34). Current clinical attempts are therefore focussed on combinational approaches, involving for example chemotherapeutic or immunotherapeutic strategies (2,35). Indeed, we and others recently demonstrated that reovirus has high potential as

a strategy to enhance the efficacy of immunotherapy by recruiting $CD8^+$ T cells to the tumor (11,36,37). Whereas stimulation of intratumoral T-cell influx represents an important pillar in the immunotherapeutic efficacy of reovirus, the dynamics of T-cell responses during reovirus therapy are not completely understood. The identification of the immunodominant $CD8^+$ T-cell epitope of reovirus enabled us to track reovirus-specific T cells and study the dynamics of this response during oncolytic virus therapy. Induction of preexisting T-cell immunity by means of vaccination did, surprisingly, not hamper viral replication, but on the contrary, empowered reovirus therapy against immunologically cold tumors.

One important consideration in the clinical use of OVs is the choice of the administration route, which is mostly focused on the efficient delivery of the OV itself to the tumor site and less on the OV-induced immune response (38,39). Interestingly, we observed that priming of reovirus-specific T cells does not depend on a specific route of administration. In fact, replication at a tumor site is not even required to mount an efficient systemic reovirus-specific T-cell response. However, intratumoral administration is required to induce an efficient influx of (reovirus-specific) $CD8^+$ T cells into the tumor. Interestingly, we found that injection of cognate peptide in the tumor was able to reactivate reovirus-specific T cells, as was previously shown for intratumoral OT-I cells recognizing the SIINFEKL peptide (40), thereby increasing the density and activation of virus-specific T-cell density in the TME.

Reovirus-specific T cells can be found throughout the body after both systemic and local reovirus administration, but only express high levels of CD69, PD1, and Tim3 after intratumorally applied reovirus or peptide. Increased cell-surface CD69 can be driven by either TCR stimulation or cytokines such as IFNα and IFNβ (41), which are both provided by the presence of replicating reovirus in the tumor. PD1 is rapidly induced on T cells following TCR-mediated activation and this expression decreases with antigen clearance (42), Tim3 is identified as being selectively expressed on IFNγ–secreting $CD4^+$ and $CD8^+$ T cells, and expression is induced after repeated TCR-stimulation (43,44). Given that all three surface markers are associated with previous antigen exposure, co-expression of these markers suggests tumor-residing reovirus-specific T cells have encountered their cognate antigen in the TME during active reovirus infection and thus recognize reovirus-infected tumor cells.

Although reovirus-specific T cells were enriched in the tumor, they did not make up the total TIL population. Since other TILs displayed similar phenotypic characteristics as reovirus-specific T cells, we hypothesize that those TILs might also be reovirus-specific but simply recognize other, yet unidentified epitopes. Identifying these epitopes and their inclusion in the vaccination strategy might further enhance SLP+Reo therapy efficacy. Tetramer-negative TILs with a much less pronounced effector phenotype might be 'bystander' T cells that are attracted to the tumor by the reovirus-induced release of chemokines and cytokines. It is not likely that tetramer-negative TILs are tumor-specific

since the administration of reovirus in both KPC3 and TC1 tumors did not induce any reactivity towards autologous tumor cells *ex vivo*. Whereas a body of literature has shown that several OVs, including reovirus, can induce tumor-specific T-cell responses (45-49), this seems to be restricted to immunogenic models with high mutational load or expression of tumor-associated or artificial antigens. Therefore, the exploitation of virus-specific T cells may represent a solution for targeting low-immunogenic tumors to which tumor-specific responses are out of the question.

Recent evidence from murine and human studies has shown that previously established antiviral T cells can also be found in tumors (40,50-53). Taking advantage of this preexisting, pathogen-specific immune cell population is an exciting new approach in the cancer immunotherapy field. This is particularly attractive in the setting of an oncolytic virus that selectively replicates in tumor cells, thereby specifically directing the virus-specific T cells to the infected tumor cells.

An important consideration when employing virus-specific T cells as anticancer effectors is that tumor cell-killing relies on the expression of the virus-derived epitopes on tumor cells. The continuous expression of viral epitopes is likely restricted by antiviral immunity (possibly by the emergence of neutralizing antibodies or innate immune responses), thereby installing a maximum level of tumor cell-killing that can be achieved by the virus-specific T cells before the virus is cleared. The emergence of antiviral immunity might also explain why continued intratumoral reovirus administration or the addition of checkpoint blockade does not improve the antitumor effect of SLP+Reo therapy. More insight into the various layers of antiviral immunity that might limit viral replication and epitope presentation in the tumor is necessary to enhance the therapeutic window of this strategy. Furthermore, it would also be interesting to study whether an initial wave of tumor cell-killing by virus-specific T cells can induce a second wave of tumor-specific T cells, so-called epitope spreading.

However, exploiting antiviral $CD8^+$ T cells also has multiple advantages over utilizing tumor-specific T cells. Antiviral T cells often display strong effector and memory responses and lack exhaustion markers including expression of CD39, which is associated with chronic antigen exposure in the tumor (51). Since antiviral T cells are generated against 'non-self' epitopes, there is no central tolerance and minimal auto-reactivity is expected. Various approaches have already demonstrated that pathogen-specific T cells can be repurposed to attack tumors (40). For instance, antibody-peptide epitope conjugates were used to redirect cytomegalovirus (CMV)-specific $CD8^+$ T cells to kill tumor cells *in vitro* and in NOD/SCID mice that were injected with expanded CMV-specific $CD8^+$ T cells and were engrafted with orthotopic human breast cancer tumors or hepatocellular carcinomas (54). Also, repurposing of severe acute respiratory syndrome-coronavirus-2 (SARS-CoV-2)-specific $CD8^+$ T-cell responses, present in a large population of coronavirus disease 2019 (COVID-19) resolvers, has been suggested as an anticancer immunotherapy approach (55).

Our approach uniquely involves the use of a non-pathogenic virus that has previously been tested in patients as an oncolytic agent with excellent safety records (34). Moreover, using an OV adds tumor-specificity to the system due to specific replication in malignant cells, thereby converting the tumor cells into target cells for the previously established virus-specific T cells. Therefore, inducing and subsequently exploiting an oncolytic virus-specific $CD8^+$ T-cell response might be considered a more generalized immunotherapy approach to combat cancer that does not require the presence of tumor-specific $CD8^+$ T cells.

DECLARATIONS

Acknowledgments. The authors thank Kees Franken en Robert Cordfunke from the protein-facility of LUMC for the generation of the Reo $\mu1_{133\text{-}140}$ tetramer to detect reovirus-specific T cells. The authors thank Vera Kemp (Department of Cell and Chemical Biology) for providing reovirus variant Jin-3 and Marit van Elsas for providing the HPV E7-derived SLP and HPV $E7_{49\text{-}57}$ tetramer. The authors gratefully acknowledge the operators of the Flow cytometry Core Facility (FCF) of the LUMC and the Animal Facility of the LUMC for their excellent support and care of the animals, respectively. The hybridoma 10F6 (reovirus μ1), developed by T. S. Dermody from the University of Pittsburgh School of Medicine, was obtained from the Developmental Studies Hybridoma Bank, created by the NICHD of the NIH and maintained at The University of Iowa, Department of Biology, Iowa City, IA 52242. Figures depicting experimental designs were created with BioRender.com.

Author contributions. Conceptualization, CG and NvM; Methodology, CG, PK, JJCvST, DvdW, RH, TvH, NvM; Formal analysis, CG; Investigation, CG, PK, JJCvST, CL, LG, MS; Resources, DvdW, RH, JMMdH; Writing – Original Draft, CG, NvM; Writing - Review & Editing, All authors; Visualization, CG; Supervision, SHvdB, TvH, NvM; Funding acquisition, SHvdB, TvH, NvM. All authors approved the final version of the manuscript.

Funding. This work was financially supported by the Dutch Cancer Society Bas Mulder Award 11056 (to NvM), a PhD fellowship from Leiden University Medical Center (to CG), and the Support Casper campaign by the Dutch foundation 'Stichting Overleven met Alvleesklierkanker' (supportcasper.nl) project number SOAK 17.04 (to SHvdB, TvH, and NvM).

Competing interests. CG, NvM, and TvH filed a patent (P335646NL) regarding the research described in this manuscript. All other authors declare no competing interests.

Ethics approval. All mouse studies were individually prepared, reviewed, approved, and registered by the institutional Animal Welfare Body of Leiden University Medical Center and carried out under project license AVD1160020187004, issued by the competent authority on animal experiments in the Netherlands (named CCD). Experiments were performed following the Dutch Act on Animal Experimentation and EU Directive 2010/63/EU ("On the protection of animals used for scientific purposes") at the animal facility of the Leiden University Medical Center (LUMC), The Netherlands.

Data availability statement. All data relevant to this study are included in the main text or the supplementary materials and are available on reasonable request.

REFERENCES

1. Groeneveldt C, van Hall T, van der Burg SH, Ten Dijke P, van Montfoort N. Immunotherapeutic Potential of TGF-β Inhibition and Oncolytic Viruses. Trends Immunol **2020**;41:406-20
2. Mahalingam D, Goel S, Aparo S, Patel Arora S, Noronha N, Tran H*, et al.* A Phase II Study of Pelareorep (REOLYSIN(®)) in Combination with Gemcitabine for Patients with Advanced Pancreatic Adenocarcinoma. Cancers (Basel) **2018**;10:160
3. Sborov DW, Nuovo GJ, Stiff A, Mace T, Lesinski GB, Benson DM*, et al.* A Phase I Trial of Single-Agent Reolysin in Patients with Relapsed Multiple Myeloma. Clinical Cancer Research **2014**;20:5946-55
4. Duncan MR, Stanish SM, Cox DC. Differential sensitivity of normal and transformed human cells to reovirus infection. J Virol **1978**;28:444-9
5. Shmulevitz M, Marcato P, Lee PWK. Unshackling the links between reovirus oncolysis, Ras signaling, translational control and cancer. Oncogene **2005**;24:7720-8
6. Smakman N, van den Wollenberg DJ, Borel Rinkes IH, Hoeben RC, Kranenburg O. Sensitization to apoptosis underlies KrasD12-dependent oncolysis of murine C26 colorectal carcinoma cells by reovirus T3D. J Virol **2005**;79:14981-5
7. Thirukkumaran CM, Nodwell MJ, Hirasawa K, Shi Z-Q, Diaz R, Luider J*, et al.* Oncolytic Viral Therapy for Prostate Cancer: Efficacy of Reovirus as a Biological Therapeutic. Cancer research **2010**;70:2435-44
8. Zhao X, Chester C, Rajasekaran N, He Z, Kohrt HE. Strategic Combinations: The Future of Oncolytic Virotherapy with Reovirus. Molecular cancer therapeutics **2016**;15:767-73
9. Samson A, Scott KJ, Taggart D, West EJ, Wilson E, Nuovo GJ*, et al.* Intravenous delivery of oncolytic reovirus to brain tumor patients immunologically primes for subsequent checkpoint blockade. Science translational medicine **2018**;10
10. Bourgeois-Daigneault MC, Roy DG, Aitken AS, El Sayes N, Martin NT, Varette O*, et al.* Neoadjuvant oncolytic virotherapy before surgery sensitizes triple-negative breast cancer to immune checkpoint therapy. Science translational medicine **2018**;10
11. Groeneveldt C, Kinderman P, van den Wollenberg DJM, van den Oever RL, Middelburg J, Mustafa DAM*, et al.* Preconditioning of the tumor microenvironment with oncolytic reovirus converts CD3-bispecific antibody treatment into effective immunotherapy. J Immunother Cancer **2020**;8:e001191
12. van den Wollenberg DJM, Dautzenberg IJC, van den Hengel SK, Cramer SJ, de Groot RJ, Hoeben RC. Isolation of reovirus T3D mutants capable of infecting human tumor cells independent of junction adhesion molecule-A. PloS One **2012**;7:e48064-e
13. Smith RE, Zweerink HJ, Joklik WK. Polypeptide components of virions, top component and cores of reovirus type 3. Virology **1969**;39:791-810
14. Fallaux FJ, Kranenburg O, Cramer SJ, Houweling A, Van Ormondt H, Hoeben RC*, et al.* Characterization of 911: a new helper cell line for the titration and propagation of early region 1-deleted adenoviral vectors. Human gene therapy **1996**;7:215-22
15. Hingorani SR, Wang L, Multani AS, Combs C, Deramaudt TB, Hruban RH*, et al.* Trp53R172H and KrasG12D cooperate to promote chromosomal instability and widely metastatic pancreatic ductal adenocarcinoma in mice. Cancer cell **2005**;7:469-83
16. Lin K-Y, Guarnieri FG, Staveley-O'Carroll KF, Levitsky HI, August JT, Pardoll DM*, et al.* Treatment of Established Tumors with a Novel Vaccine That Enhances Major Histocompatibility Class II Presentation of Tumor Antigen. Cancer Res **1996**;56:21-6
17. Winzler C, Rovere P, Rescigno M, Granucci F, Penna G, Adorini L*, et al.* Maturation Stages of Mouse Dendritic Cells in Growth Factor–dependent Long-Term Cultures. Journal of Experimental Medicine **1997**;185:317-28
18. van Hall T, van Bergen J, van Veelen PA, Kraakman M, Heukamp LC, Koning F*, et al.* Identification of a Novel Tumor-Specific CTL Epitope Presented by RMA, EL-4, and MBL-2 Lymphomas Reveals Their Common Origin. J Immunol **2000**;165:869-77

19. Belkina AC, Ciccolella CO, Anno R, Halpert R, Spidlen J, Snyder-Cappione JE. Automated optimized parameters for T-distributed stochastic neighbor embedding improve visualization and analysis of large datasets. Nature Communications **2019**;10:5415
20. van den Wollenberg DJ, Dautzenberg IJ, van den Hengel SK, Cramer SJ, de Groot RJ, Hoeben RC. Isolation of reovirus T3D mutants capable of infecting human tumor cells independent of junction adhesion molecule-A. PLoS One **2012**;7:e48064
21. Mijatovic-Rustempasic S, Tam KI, Kerin TK, Lewis JM, Gautam R, Quaye O, *et al.* Sensitive and specific quantitative detection of rotavirus A by one-step real-time reverse transcription-PCR assay without antecedent double-stranded-RNA denaturation. Journal of clinical microbiology **2013**;51:3047-54
22. Dupont WD, Plummer WD, Jr. Power and sample size calculations. A review and computer program. Controlled clinical trials **1990**;11:116-28
23. Murphy JP, Kim Y, Clements DR, Konda P, Schuster H, Kowalewski DJ, *et al.* Therapy-Induced MHC I Ligands Shape Neo-Antitumor CD8 T Cell Responses during Oncolytic Virus-Based Cancer Immunotherapy. J Proteome Res **2019**;18:2666-75
24. van de Merbel AF, van der Horst G, van der Mark MH, Bots STF, van den Wollenberg DJM, de Ridder CMA, *et al.* Reovirus mutant jin-3 exhibits lytic and immune-stimulatory effects in preclinical human prostate cancer models. Cancer Gene Ther **2021**
25. Woopen C, Straub T, Schweier O, Aichele U, Düker K, Boehm T, *et al.* Immunological tolerance to LCMV antigens differently affects control of acute and chronic virus infection in mice. European Journal of Immunology **2018**;48:120-7
26. Belz GT, Xie W, Altman JD, Doherty PC. A Previously Unrecognized H-2Db-Restricted Peptide Prominent in the Primary Influenza A Virus-Specific $CD8^+$ T-Cell Response Is Much Less Apparent following Secondary Challenge. J Virol **2000**;74:3486-93
27. Schreiber L-M, Urbiola C, Das K, Spiesschaert B, Kimpel J, Heinemann F, *et al.* The lytic activity of VSV-GP treatment dominates the therapeutic effects in a syngeneic model of lung cancer. British Journal of Cancer **2019**;121:647-58
28. Noubade R, Majri-Morrison S, Tarbell KV. Beyond cDC1: Emerging Roles of DC Crosstalk in Cancer Immunity. Front Immunol **2019**;10
29. Desai P, Tahiliani V, Abboud G, Stanfield J, Salek-Ardakani S. Batf3-Dependent Dendritic Cells Promote Optimal CD8 T Cell Responses against Respiratory Poxvirus Infection. J Virol **2018**;92
30. Davenport BJ, Bullock C, McCarthy MK, Hawman DW, Murphy KM, Kedl RM, *et al.* Chikungunya Virus Evades Antiviral $CD8^+$ T Cell Responses To Establish Persistent Infection in Joint-Associated Tissues. J Virol **2020**;94
31. Dai P, Wang W, Yang N, Serna-Tamayo C, Ricca JM, Zamarin D, *et al.* Intratumoral delivery of inactivated modified vaccinia virus Ankara (iMVA) induces systemic antitumor immunity via STING and Batf3-dependent dendritic cells. Sci Immunol **2017**;2:eaal1713
32. Hildner K, Edelson BT, Purtha WE, Diamond M, Matsushita H, Kohyama M, *et al.* Batf3 Deficiency Reveals a Critical Role for $CD8\alpha^+$ Dendritic Cells in Cytotoxic T Cell Immunity. Science **2008**;322:1097-100
33. van Dinther D, Veninga H, Iborra S, Borg EGF, Hoogterp L, Olesek K, *et al.* Functional CD169 on Macrophages Mediates Interaction with Dendritic Cells for $CD8^+$ T Cell Cross-Priming. Cell Rep **2018**;22:1484-95
34. Müller L, Berkeley R, Barr T, Ilett E, Errington-Mais F. Past, Present and Future of Oncolytic Reovirus. Cancers **2020**;12:3219
35. Mahalingam D, Wilkinson GA, Eng KH, Fields P, Raber P, Moseley JL, *et al.* Pembrolizumab in Combination with the Oncolytic Virus Pelareorep and Chemotherapy in Patients with Advanced Pancreatic Adenocarcinoma: A Phase Ib Study. Clin Cancer Res **2020**;26:71-81
36. Samson A, Scott KJ, Taggart D, West EJ, Wilson E, Nuovo GJ, *et al.* Intravenous delivery of oncolytic reovirus to brain tumor patients immunologically primes for subsequent checkpoint blockade. Sci Transl Med **2018**;10:eaam7577

37. Mostafa AA, Meyers DE, Thirukkumaran CM, Liu PJ, Gratton K, Spurrell J*, et al.* Oncolytic Reovirus and Immune Checkpoint Inhibition as a Novel Immunotherapeutic Strategy for Breast Cancer. Cancers (Basel) **2018**;10
38. Macedo N, Miller DM, Haq R, Kaufman HL. Clinical landscape of oncolytic virus research in 2020. Journal for ImmunoTherapy of Cancer **2020**;8:e001486
39. Kaufman HL, Bommareddy PK. Two roads for oncolytic immunotherapy development. Journal for ImmunoTherapy of Cancer **2019**;7:26
40. Rosato PC, Wijeyesinghe S, Stolley JM, Nelson CE, Davis RL, Manlove LS*, et al.* Virus-specific memory T cells populate tumors and can be repurposed for tumor immunotherapy. Nature Communications **2019**;10:567
41. Shiow LR, Rosen DB, Brdičková N, Xu Y, An J, Lanier LL*, et al.* CD69 acts downstream of interferon-α/β to inhibit S1P1 and lymphocyte egress from lymphoid organs. Nature **2006**;440:540-4
42. Chikuma S, Terawaki S, Hayashi T, Nabeshima R, Yoshida T, Shibayama S*, et al.* PD-1-Mediated Suppression of IL-2 Production Induces CD8$^+$ T Cell Anergy In Vivo. J Immunol **2009**;182:6682-9
43. Monney L, Sabatos CA, Gaglia JL, Ryu A, Waldner H, Chernova T*, et al.* Th1-specific cell surface protein Tim-3 regulates macrophage activation and severity of an autoimmune disease. Nature **2002**;415:536-41
44. Borst L, Sluijter M, Sturm G, Charoentong P, Santegoets SJ, van Gulijk M*, et al.* NKG2A is a late immune checkpoint on CD8 T cells and marks repeated stimulation and cell division. Int J Cancer **2021**:1-17
45. Diaz RM, Galivo F, Kottke T, Wongthida P, Qiao J, Thompson J*, et al.* Oncolytic Immunovirotherapy for Melanoma Using Vesicular Stomatitis Virus. Cancer Res **2007**;67:2840-8
46. Wang G, Kang X, Chen KS, Jehng T, Jones L, Chen J*, et al.* An engineered oncolytic virus expressing PD-L1 inhibitors activates tumor neoantigen-specific T cell responses. Nature Communications **2020**;11:1395
47. Woller N, Gürlevik E, Fleischmann-Mundt B, Schumacher A, Knocke S, Kloos AM*, et al.* Viral Infection of Tumors Overcomes Resistance to PD-1-immunotherapy by Broadening Neoantigenome-directed T-cell Responses. Molecular therapy : the journal of the American Society of Gene Therapy **2015**;23:1630-40
48. Prestwich RJ, Ilett EJ, Errington F, Diaz RM, Steele LP, Kottke T*, et al.* Immune-mediated antitumor activity of reovirus is required for therapy and is independent of direct viral oncolysis and replication. Clin Cancer Res **2009**;15:4374-81
49. Brown MC, Holl EK, Boczkowski D, Dobrikova E, Mosaheb M, Chandramohan V*, et al.* Cancer immunotherapy with recombinant poliovirus induces IFN-dominant activation of dendritic cells and tumor antigen–specific CTLs. Sci Transl Med **2017**;9:eaan4220
50. Erkes DA, Smith CJ, Wilski NA, Caldeira-Dantas S, Mohgbeli T, Snyder CM. Virus-Specific CD8$^+$ T Cells Infiltrate Melanoma Lesions and Retain Function Independently of PD-1 Expression. J Immunol **2017**;198:2979-88
51. Simoni Y, Becht E, Fehlings M, Loh CY, Koo SL, Teng KWW*, et al.* Bystander CD8$^+$ T cells are abundant and phenotypically distinct in human tumour infiltrates. Nature **2018**;557:575-9
52. Saini SK, Ørskov AD, Bjerregaard AM, Unnikrishnan A, Holmberg-Thydén S, Borch A*, et al.* Human endogenous retroviruses form a reservoir of T cell targets in hematological cancers. Nat Commun **2020**;11:5660
53. Bentzen AK, Marquard AM, Lyngaa R, Saini SK, Ramskov S, Donia M*, et al.* Large-scale detection of antigen-specific T cells using peptide-MHC-I multimers labeled with DNA barcodes. Nature Biotechnology **2016**;34:1037-45
54. Millar DG, Ramjiawan RR, Kawaguchi K, Gupta N, Chen J, Zhang S*, et al.* Antibody-mediated delivery of viral epitopes to tumors harnesses CMV-specific T cells for cancer therapy. Nature Biotechnology **2020**;38:420-5
55. Gujar S, Pol JG, Kim Y, Kroemer G. Repurposing CD8$^+$ T cell immunity against SARS-CoV-2 for cancer immunotherapy: a positive aspect of the COVID-19 pandemic? Oncoimmunology **2020**;9:1794424

SUPPLEMENTARY FIGURES

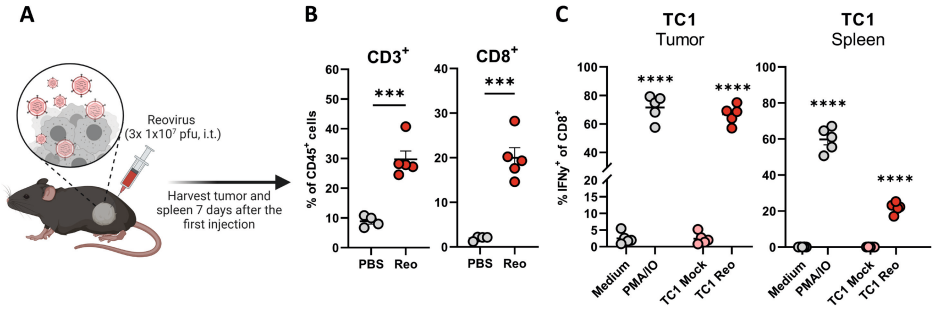

Figure S1. Local and systemic presence of reovirus-specific T cells in the TC1 model. (**A**) Design of the experiment described in B-C. Mice (n=5–8/group) with established TC1 tumors were intratumorally (i.t.) injected with reovirus (10^7 plaque-forming units (pfu)) on 3 consecutive days. Mice were sacrificed 7 days after the first reovirus injection for ex vivo analysis of tumors and spleens. (**B**) Frequency of $CD3^+$ and $CD8^+$ T cells within the total $CD45^+$ immune cell population in TC1 tumors after reovirus administration. (**C**) Frequency of interferon γ $(IFNγ)^+$ cells within the intratumoral and splenic $CD8^+$ T-cell population as measured with intracellular cytokine staining. Single-cell suspensions (n=5/group) were cocultured with indicated targets for 6 hours. Medium was used as negative control and PMA/ionomycin (IO) was used as positive control. Data are presented as mean±SEM. Statistical tests used: (B): unpaired t-test between PBS and Reo groups. (C): ordinary one-way analysis of variance (ANOVA) with Dunnett's post hoc test. Statistical difference was compared to medium control group. Significance levels: ***p<0.001 and ****p<0.0001.

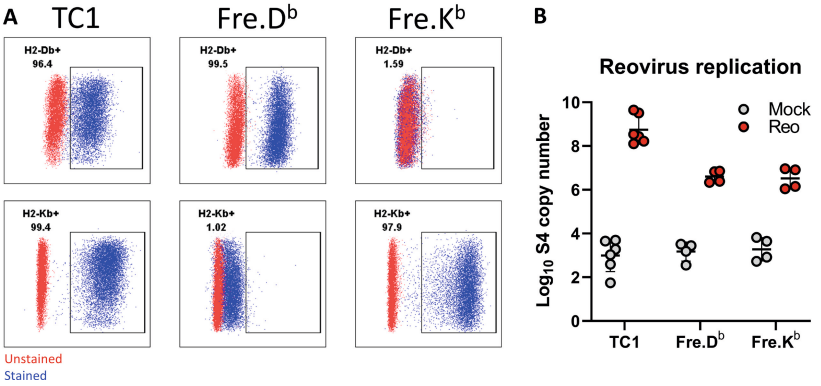

Figure S2. MHC class I expression and reovirus replication in TC1, Fre.K^b and Fre.D^b cells. (**A**) K^b and D^b expression on TC1, Fre.K^b and Fre.D^b cells as measured with flow cytometry. (**B**) Reovirus genomic segment 4 (S4) copy number in TC1, Fre.K^b and Fre.D^b cells after reovirus infection. Cells ($1.5x10^5$/well) were infected with multiplicities of infection (MOI)=10. Samples (n=2-3) were harvested 24 hours after infection and reovirus S4 copy numbers were determined by quantitative reverse transcription PCR (RT-qPCR). Individual data points represent 2-3 biological duplicates with each 2 technical replicates.

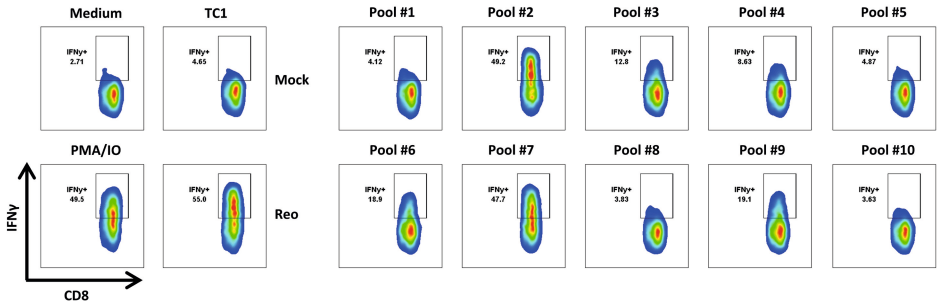

Figure S3. T-cell recognition of positive peptide pools. (**A**) Frequency of interferon γ (IFNγ)$^+$ cells within the reovirus-specific T-cell bulk as measured with intracellular cytokine staining. T cells were cocultured with peptide pools (1 µg/mL for each peptide) for 6 hours. Medium was used as negative control and phorbol 12-myristate 13-acetate (PMA)/ionomycin (IO) was used as positive control.

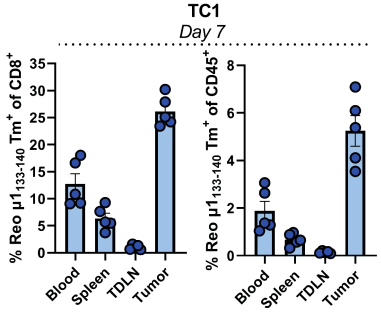

Figure S4. Frequency and distribution of reovirus-specific T cells in TC1-bearing mice. Quantification of Tm$^+$ cells out of CD8$^+$T cells and total CD45$^+$ immune cell population in indicated organs on day 7 after the first intratumoral reovirus injection in mice bearing established TC1 tumors. Data are presented as mean±SEM.

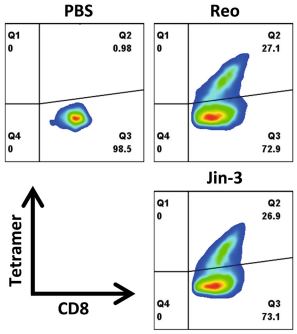

Figure S5. Reovirus-specific T cells in tumors after intratumoral Reo or Jin-3 administration. Representative flow cytometry plots of Tm$^+$ CD8$^+$T cells in tumors injected with Reo or Jin-3 according to the schedule described in Figure 2A. Tumors were harvested on day 7 after the first intratumoral reovirus injection.

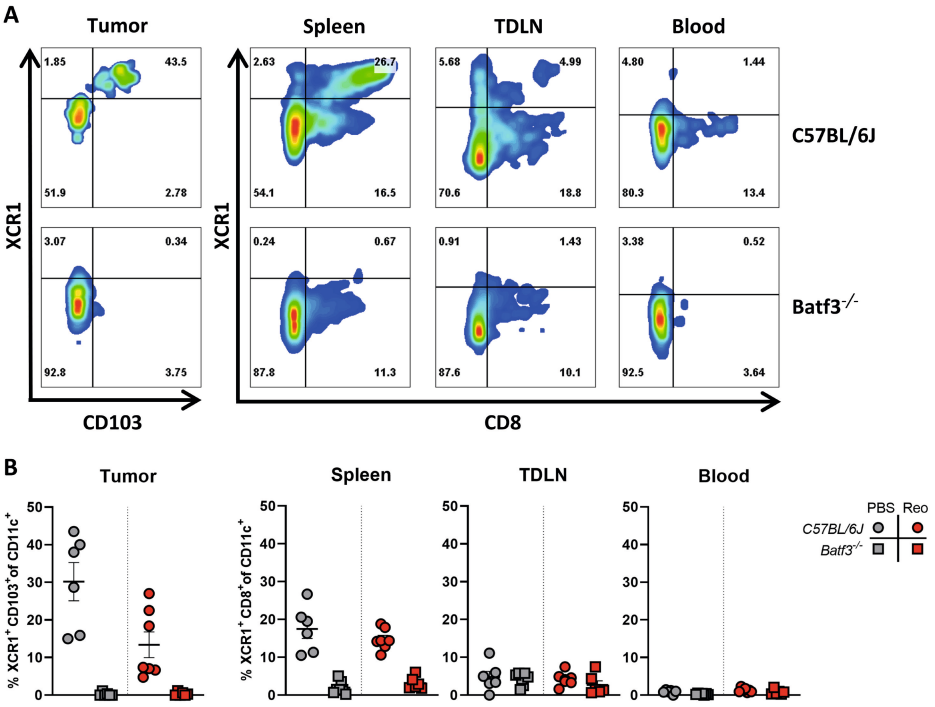

Figure S6. cDC1 absence in *Batf3*$^{-/-}$ mice. (**A**) Flow cytometry plots of cDC1s (characterized by XCR1 and CD103 expression in tumors, and XCR1 and CD8 expression in other organs) in tumors, spleens, tumor-draining lymph nodes (TDLN), and blood of KPC3-bearing, PBS-treated C57BL/6J mice or *Batf3*$^{-/-}$ mice. (**B**) Quantification of cDC1s (n=5-7/group). All data are presented as mean±SEM.

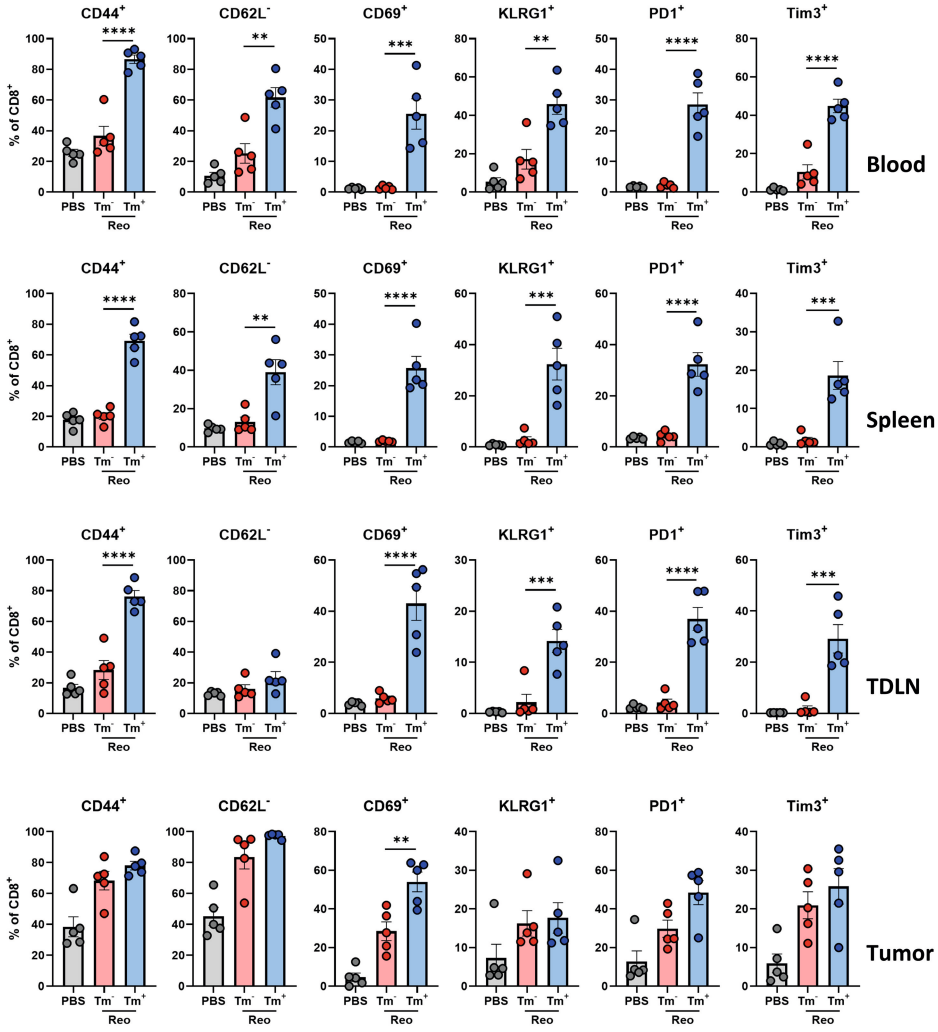

Figure S7. Phenotype of reovirus-specific T cells on day 12. Expression of activation markers on Tm^- or Tm^+ $CD8^+$ T cells in blood, spleen, tumor-draining lymph node (TDLN), and tumor, 12 days after the first intratumoral reovirus injection. All data are presented as mean±SEM. Statistical tests used: (A): ordinary one-way analysis of variance (ANOVA) with Tukey's post hoc test. Significance levels: *p<0.05, **p<0.01, ***p<0.001, and ****p<0.0001.

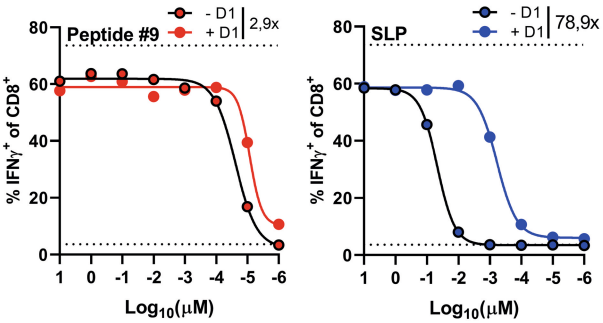

Figure S8. Processing of SLPs by D1 cells and activation of reovirus-specific T cells. Frequency of IFNγ⁺ cells within reovirus-specific T-cell bulk after coculture with peptide #9 or the SLP (10 μM to 10 pM). Peptides were added directly or in the context of D1 cells as antigen-presenting cells and incubated with T cells for 6 hours. Before coculture with T cells, D1 cells were pre-incubated for 1 hour with peptide #9 or SLP after which lipopolysaccharide (LPS; 10 μg/mL) was added to each well for an additional 23 hours.

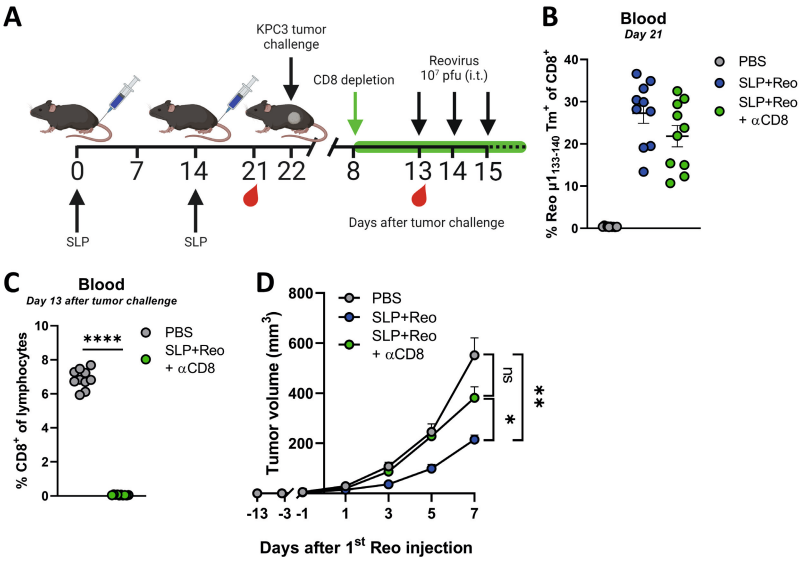

Figure S9. Depletion of CD8 T cells diminishes SLP+Reo effect. (**A**) Design of the experiment described in (B-D). Mice were vaccinated on days 0 and/or 14 by injecting 100 μg SLP together with 20 μg CpG in the tail-base region. On day 22, KPC3 tumor challenge was performed. 8 days after KPC3 tumor inoculation, CD8⁺ T-cell depletion was initiated (Clone 2.42, 50 μg intraperitoneal). Mice with established KPC3 tumors were intratumorally (i.t.) injected with reovirus (10^7 plaque-forming units (pfu)) on days 13, 14, and 15 after the tumor challenge. (**B**) Frequency of Reo $\mu1_{133\text{-}140}$ Tm⁺ cells within CD8⁺ T cells after vaccination. (**C**) Frequency of CD8⁺ T cells in blood after CD8⁺ T-cell depletion. (**D**) Average growth curves of mice (n=10/group) receiving indicated treatments. All data are presented as mean±SEM. Statistical tests used: (C) unpaired t-test. (D): ordinary two-way ANOVA with Tukey's post hoc test. Significance levels: *p<0.05, **p<0.01, ****p<0.0001. The control group is shared with Figure S12.

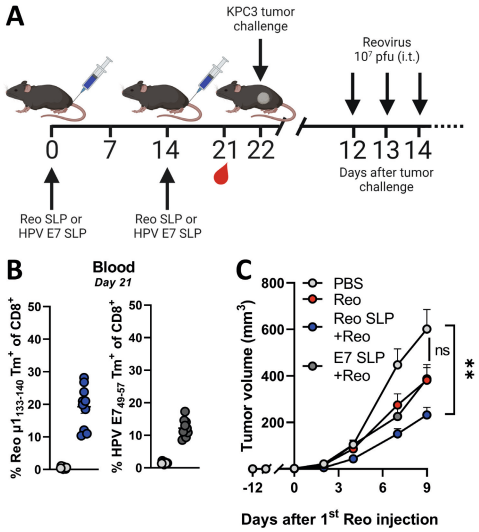

Figure S10. Irrelevant SLP vaccination impairs the antitumor efficacy of SLP+Reo therapy. (**A**) Design of the experiment described in (B-C). Mice were vaccinated with an SLP containing the reovirus epitope (Reo SLP) or an irrelevant SLP containing an HPV E7 epitope (E7 SLP) on days 0 and 14 by injecting 100 μg SLP together with 20 μg CpG in the tail-base region. On day 22, KPC3 tumor challenge was performed. Mice with established KPC3 tumors were intratumorally (i.t.) injected with reovirus (10^7 plaque-forming units (pfu)) on days 12, 13, and 14 after the tumor challenge. (**B**) Frequency of Reo $\mu1_{133-140}$ or HPV16 $E7_{49-57}$ Tm^+ cells within $CD8^+$ T cells after vaccination. (**C**) Average growth curves of mice (n=10/group) receiving indicated treatments. All data are presented as mean±SEM. Statistical tests used: (C): ordinary two-way ANOVA with Tukey's post hoc test. Significance level: **p<0.01. Control groups are shared with Figure S13 and Figure 8.

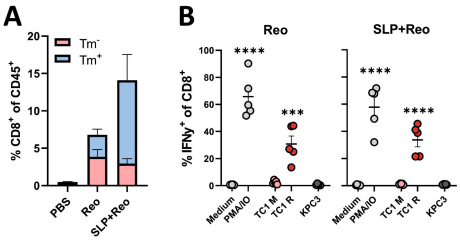

Figure S11. Presence of reovirus-specific but not tumor-specific T cells in end-stage tumors after SLP+Reo therapy. (**A**) Separation of Tm^+ cells from Tm^- cells within the total $CD8^+$ T cell population of end-stage KPC3 tumors after Reo or SLP+Reo therapy. (**B**) Frequency of interferon γ $(IFNγ)^+$ cells within the intratumoral $CD8^+$ T-cell population of end-stage KPC3 tumors that received Reo or SLP+Reo therapy. Single-cell suspensions (n=5/group) were cocultured with indicated targets. PMA/ionomycin (IO) was used as a positive control, and the irrelevant cell line TC1 was used as target cell line for reovirus infection. Data are presented as mean±SEM. Statistical tests used: (B): ordinary one-way analysis of variance (ANOVA) with Dunnett's post hoc test. Statistical difference was compared to medium control group. Significance level: ****p<0.0001.

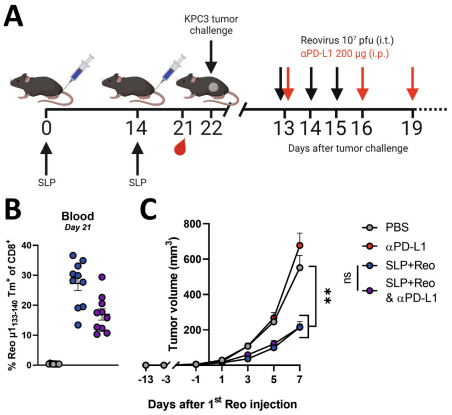

Figure S12. The antitumor effect of SLP+Reo therapy cannot be improved by the addition of αPD-L1 therapy. (**A**) Design of the experiment described in (B-C). Mice were vaccinated with an SLP containing the reovirus epitope on days 0 and 14 by injecting 100 μg SLP together with 20 μg CpG in the tail-base region. On day 22, KPC3 tumor challenge was performed. Mice with established KPC3 tumors were intratumorally (i.t.) injected with reovirus (10^7 plaque-forming units (pfu)) on days 13, 14, and 15 after the tumor challenge. αPD-L1 was administered intraperitoneally (i.p.) on days 14, 16, and 19. (**B**) Frequency of Reo $\mu1_{133\text{-}140}$ Tm^+ cells within $CD8^+$ T cells after vaccination. (**C**) Average growth curves of mice (n=10/group) receiving indicated treatments. All data are presented as mean±SEM. Statistical tests used: (C): ordinary two-way ANOVA with Tukey's post hoc test. Significance level: **p<0.01. The control group is shared with Figure S9.

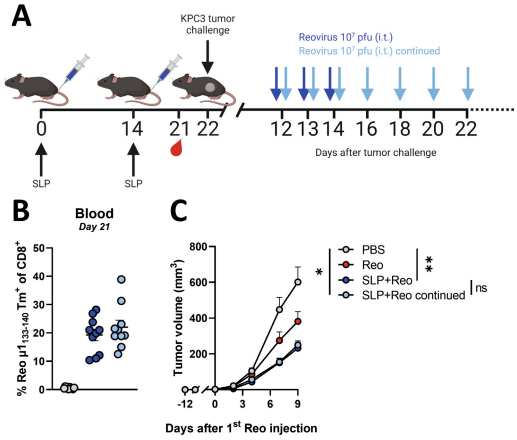

Figure S13. Continuation of intratumoral reovirus administration does not improve the antitumor effect of SLP+Reo therapy. (**A**) Design of the experiment described in (B-C). Mice were vaccinated with an SLP containing the reovirus epitope on days 0 and 14 by injecting 100 μg SLP together with 20 μg CpG in the tail-base region. On day 22, KPC3 tumor challenge was performed. Mice with established KPC3 tumors were intratumorally (i.t.) injected with reovirus (10^7 plaque-forming units (pfu)) on days 12, 13, and 14 after the tumor challenge. One group continued to receive intratumoral reovirus injections every 2 days after day 14. (**B**) Frequency of Reo $\mu1_{133\text{-}140}$ Tm^+ cells within $CD8^+$ T cells after vaccination. (**C**) Average growth curves of mice (n=10/group) receiving indicated treatments. All data are presented as mean±SEM. Statistical tests used: (C): ordinary two-way ANOVA with Tukey's post hoc test. Significance levels: *p<0.05 and **p<0.01. Control groups are shared with Figure S10 and Figure 8.

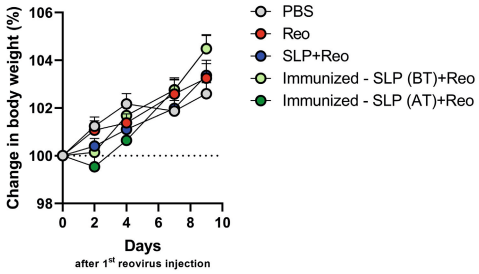

Figure S14. Boosting the reovirus-specific T-cell response does not affect body weight.
Increase in body weight (%) starting from the moment of the first intratumoral reovirus injection.

SUPPLEMENTARY TABLES

Table S1. List of antibodies used for flow cytometric analysis.

	Marker	*Clone*	*Fluorochrome*	*Supplier*
Lymphoid panel	CD45.2	104	FITC	eBioscience
	CD3	145-2C11	PE-CF594	BD Biosciences
	CD8α	53-6.7	Alexa Fluor 700	eBioscience
	Reo $\mu1_{133-140}$ tetramer		APC	In house
	HPV $E7_{49-57}$ tetramer		PE	In house
	CD44	IM-7	BV785	BioLegend
	CD62L	MEL-14	BV421	BioLegend
	NK1.1	Pk136	BV650	BD Biosciences
	PD-1	29F.1A12	APC-Cy7	BioLegend
	Tim3	RMT3-23	PE	BioLegend
	NKG2A	16A11	PE	eBioscience
	KLRG-1	2F1	PE-Cy7	eBioscience
	CD103	2E7	BV711	BioLegend
	CD69	H1.2F3	BV605	BioLegend
Myeloid panel	CD45.2	104	FITC	BioLegend
	CD11b	M1/70	PE-Cy7	BioLegend
	CD11c	N418	APC-Cy7	BioLegend
	CD8α	53-6.7	Alexa Fluor 700	eBioscience
	CD103	2E7	BV711	BioLegend
	XCR1	ZET	PE	BioLegend
	CD4	RM4-5	APC	BioLegend
Intracellular T-cell activation panel	CD45.2	104	FITC	eBioscience
	CD3	145-2C11	PE-CF594	BD Biosciences
	CD8α	53-6.7	Alexa Fluor 700	eBioscience
	IFNγ	XMG1.2	APC	BioLegend

Table S2. GenBank accession numbers of Reovirus Type 3 Dearing isolate R124 segments.

Segment	*GenBank accession number*	*Link*
Segment S1	GU991665	https://www.ncbi.nlm.nih.gov/nuccore/325112732
Segment S2	GU991666	https://www.ncbi.nlm.nih.gov/nuccore/325112734
Segment S3	GU991667	https://www.ncbi.nlm.nih.gov/nuccore/325112736
Segment S4	GU991668	https://www.ncbi.nlm.nih.gov/nuccore/325112738
Segment M1	GU991662	https://www.ncbi.nlm.nih.gov/nuccore/325112726
Segment M2	GU991663	https://www.ncbi.nlm.nih.gov/nuccore/406601112
Segment M3	GU991664	https://www.ncbi.nlm.nih.gov/nuccore/325112730
Segment L1	GU991659	https://www.ncbi.nlm.nih.gov/nuccore/325112720
Segment L2	GU991660	https://www.ncbi.nlm.nih.gov/nuccore/325112722
Segment L3	GU991661	https://www.ncbi.nlm.nih.gov/nuccore/325112724

Table S3. Predicted H2-K^b reovirus epitopes tested in intracellular cytokine staining.

N	*Peptide*	*Allele*	*nM*	*Rank*	*Segment*	
1	ISDVYAPL	H-2-K^b	4.2	0.010	M1	Pool #1
2	SAVLFSPL	H-2-K^b	3.9	0.010	L3	
3	MVYDYSEL	H-2-K^b	5.9	0.015	S4	
4	SSYAWFIL	H-2-K^b	6.0	0.015	L1	
5	ISPAHAYL	H-2-K^b	7.4	0.020	M3	
6	LMYKYMPI	H-2-K^b	6.6	0.020	L2	Pool #2
7	INFVSAML	H-2-K^b	8.3	0.025	M3	
8	LSLNFVTGL	H-2-K^b	10.5	0.030	S1	
9	VSPKYSDL	H-2-K^b	10.9	0.030	M2	
10	VSYSGSGL	H-2-K^b	13.3	0.040	S1	
11	ISITSAAL	H-2-K^b	14.0	0.040	M3	Pool #3
12	AVQLFRPL	H-2-K^b	14.3	0.040	L2	
13	VAVQLFRPL	H-2-K^b	14.2	0.040	L2	
14	QGYYMAQL	H-2-K^b	14.1	0.040	L1	
15	VNPYYRLM	H-2-K^b	17.4	0.050	L2	
16	SNQAFYDLL	H-2-K^b	15.9	0.050	L2	Pool #4
17	VGYLQYPM	H-2-K^b	17.2	0.050	L1	
18	LNANYFGHL	H-2-K^b	18.6	0.060	M1	
19	KSRLRYLPL	H-2-K^b	20.8	0.060	L2	
20	MSIPYQHV	H-2-K^b	23.9	0.070	M3	
21	VSIRAPRL	H-2-K^b	21.5	0.070	M1	Pool #5
22	AAFLFKTV	H-2-K^b	25.8	0.080	S2	
23	WSFVYWGL	H-2-K^b	25.6	0.080	L1	
24	HSYSSFSKL	H-2-K^b	25.4	0.080	L1	
25	SMFKHHVKL	H-2-K^b	25.2	0.080	L1	
26	STHLWSPL	H-2-K^b	29.1	0.090	L3	Pool #6
27	MTPMYLQQL	H-2-K^b	30.5	0.090	L3	
28	IMGVFFNGV	H-2-K^b	30.1	0.090	L1	
29	ITVNPYYRL	H-2-K^b	32.3	0.100	L2	
30	KIFQAAQL	H-2-K^b	33.0	0.100	L1	
31	ITWDFFLSV	H-2-K^b	33.9	0.100	L1	Pool #7
32	SPNYRFRQSM	H-2-K^b	39.7	0.125	S1	
33	TVVNYVQL	H-2-K^b	39.6	0.125	M2	
34	VSPKYSDLL	H-2-K^b	42.7	0.125	M2	
35	KAFMTLANM	H-2-K^b	41.6	0.125	L3	
36	STRKYFAQTL	H-2-K^b	36.2	0.125	L1	Pool #8
37	CSAVLFSPL	H-2-K^b	43.6	0.150	L3	
38	VSIRGRWMARL	H-2-K^b	49.7	0.150	L3	
39	LSYDLRWTRL	H-2-K^b	49.4	0.150	L2	
40	SDYKFMYM	H-2-K^b	51.5	0.150	L1	

Table S3. Continued.

N	*Peptide*	*Allele*	*nM*	*Rank*	*Segment*	
41	IAPMRFVL	H-2-K^b	53.2	0.175	M2	Pool #9
42	SNQAFYDL	H-2-K^b	61.7	0.175	L2	
43	HFYRYETL	H-2-K^b	52.8	0.175	L2	
44	SRLRYLPL	H-2-K^b	62.1	0.175	L2	
45	LMYKYMPIM	H-2-K^b	57.3	0.175	L2	
46	MNYYLLATF	H-2-K^b	66.9	0.200	M2	Pool #10
47	AGWLYNGV	H-2-K^b	70.5	0.200	L3	
48	TWYLAAARM	H-2-K^b	68.4	0.200	L1	

Table S4. List of primers used for RT-qPCR analysis.

Gene	*Forward*	*Reverse*
S4Q	5′-CGCTTTTGAAGGTCGTGTATCA-3′	5′-CTGGCTGTGCTGAGATTGTTTT-3′
Ifit-1	5′-CTGGACAAGGTGGAGAAGGT-3′	5′-AGGGTTTTCTGGCTCCACTT-3′
Ifit-2	5′-TGCTCTTGACTGTGAGGAGG-3′	5′-ATCCAGACGGTAGTTCGCAA-3′
Ifit-3	5′-GTGCAACCAGGTCGAACATT-3′	5′- AGGTGACCAGTCGACGAATT-3′
Irf7	5′-GACCGTGTTTACGAGGAACC-3′	5′-GCTGTACAGGAACACGCATC-3′
Isg15	5′-GGAACGAAAGGGGCCACAGCA-3′	5′-CCTCCATGGGCCTTCCCTCGA-3′
Oas1b	5′-AGCATGAGAGACGTTGTGGA-3′	5′-GCGTAGAATTGTTGGTTAGGCT-3′
Ddx58	5′-AAGGCCACAGTTGATCCAAA-3′	5′-TTGGCCAGTTTTCCTTGTCG-3′
Cxcl9	5′-TGGAGTTCGAGGAACCCTAGT-3′	5′-AGGCAGGTTTGATCTCCGTT-3′
Cxcl10	5′-ACGAACTTAACCACCATCT-3′	5′-TAAACTTTAACTACCCATTGATACATA-3′
Mx1	5′-GATGGTCCAAACTGCCTTCG-3′	5′-TTGTAAACCTGGTCCTGGCA-3′
β2M	5′-CTCGGTGACCCTGGTCTTT-3′	5′-CCGTTCTTCAGCATTTGGAT-3′
Mzt2	5′-TCGGTGCCCATATCTCTGTC-3′	5′-CTGCTTCGGGAGTTGCTTTT-3′
Ptp4a2	5′-AGCCCCTGTGGAGATCTCTT-3′	5′-AGCATCACAAACTCGAACCA-3′